Since January 2020 Elsevier has created a COVID-19 resource centre with free information in English and Mandarin on the novel coronavirus COVID-19. The COVID-19 resource centre is hosted on Elsevier Connect, the company's public news and information website.

Article

Immunity

Immunodeficiency syndromes differentially impact the functional profile of SARS-CoV-2-specific T cells elicited by mRNA vaccination

Highlights

- Single-cell map of SARS-CoV-2-specific T cell functions after mRNA vaccination
- Impaired T cell function in solid-organ transplant and chronic leukemia patients
- Individuals with an inherited lack of mature B cells possess functional T cells
- Persisting memory $CD8^+$ T cells display a stem-like effector-memory $CD45RA^+$ phenotype

Authors

Yu Gao, Curtis Cai, David Wullimann, ..., Hans-Gustaf Ljunggren, Soo Aleman, Marcus Buggert

Correspondence

marcus.buggert@ki.se

In brief

Many immunocompromised individuals respond poorly to mRNA vaccination and are at higher risk of developing severe COVID-19. Gao and Cai et al. provide the single-cell landscape of SARS-CoV-2-specific T cells after mRNA vaccination and observe that the functional quality of memory T cell responses varies considerably across different immunodeficiency syndromes.

Gao et al., 2022, Immunity *55*, 1732–1746
September 13, 2022
https://doi.org/10.1016/j.immuni.2022.07.005

CellPress

CellPress
OPEN ACCESS

Immunity

Article

Immunodeficiency syndromes differentially impact the functional profile of SARS-CoV-2-specific T cells elicited by mRNA vaccination

Yu Gao,[1,19] Curtis Cai,[1,19] David Wullimann,[1] Julia Niessl,[1] Olga Rivera-Ballesteros,[1] Puran Chen,[1] Joshua Lange,[1] Angelica Cuapio,[1] Ola Blennow,[2,3,4] Lotta Hansson,[5,6] Stephan Mielke,[7,8] Piotr Nowak,[2,9,10] Jan Vesterbacka,[2,9] Mira Akber,[1] Andre Perez-Potti,[1] Takuya Sekine,[1] Thomas R. Müller,[1] Caroline Boulouis,[1] Tobias Kammann,[1] Tiphaine Parrot,[1] Jagadeeswara Rao Muvva,[1] Michal Sobkowiak,[11] Katie Healy,[11] Gordana Bogdanovic,[12] Sandra Muschiol,[12,13] Gunnar Söderdahl,[3,4] Anders Österborg,[5,6] Fredrika Hellgren,[14] Alba Grifoni,[15] Daniela Weiskopf,[15] Alessandro Sette,[15,16] Karin Loré,[14] Margaret Sällberg Chen,[11] Per Ljungman,[8,17] Johan K. Sandberg,[1] C.I. Edvard Smith,[2,8] Peter Bergman,[2,18] Hans-Gustaf Ljunggren,[1] Soo Aleman,[2,9] and Marcus Buggert[1,20,*]

[1]Department of Medicine Huddinge, Center for Infectious Medicine, Karolinska Institutet, Stockholm, Sweden
[2]Department of Infectious Diseases, Karolinska University Hospital, Stockholm, Sweden
[3]Department of Transplantation, Karolinska University Hospital, Stockholm, Sweden
[4]Department of Clinical Science, Intervention and Technology, Karolinska Institutet, Stockholm, Sweden
[5]Department of Hematology, Karolinska University Hospital, Stockholm, Sweden
[6]Department of Oncology-Pathology, Karolinska Institutet, Stockholm, Sweden
[7]Department of Laboratory Medicine, Biomolecular and Cellular Medicine, Karolinska Institutet, Stockholm, Sweden
[8]Department of Cellular Therapy and Allogeneic Stem Cell Transplantation (CAST), Karolinska University Hospital Huddinge, Stockholm, Sweden
[9]Department of Medicine Huddinge, Infectious Diseases, Karolinska Institute, Stockholm, Sweden
[10]Laboratory for Molecular Infection Medicine Sweden MIMS, Umeå University, Umeå, Sweden
[11]Department of Dental Medicine, Karolinska Institutet, Stockholm, Sweden
[12]Department of Clinical Microbiology, Karolinska University Hospital, Stockholm, Sweden
[13]Department of Microbiology, Tumor and Cell Biology, Karolinska Institutet, Stockholm, Sweden
[14]Department of Medicine Solna, Karolinska Institutet, Karolinska University Hospital, Stockholm, Sweden
[15]Center for Infectious Disease and Vaccine Research, La Jolla Institute for Immunology, La Jolla, CA, USA
[16]Department of Medicine, Division of Infectious Diseases and Global Public Health, University of California, San Diego (UCSD), La Jolla, CA, USA
[17]Department of Medicine Huddinge, Hematology, Karolinska Institutet, Stockholm, Sweden
[18]Department of Laboratory Medicine, Clinical Microbiology, Karolinska Institutet, Stockholm, Sweden
[19]These authors contributed equally
[20]Lead contact
*Correspondence: marcus.buggert@ki.se
https://doi.org/10.1016/j.immuni.2022.07.005

SUMMARY

Many immunocompromised patients mount suboptimal humoral immunity after SARS-CoV-2 mRNA vaccination. Here, we assessed the single-cell profile of SARS-CoV-2-specific T cells post-mRNA vaccination in healthy individuals and patients with various forms of immunodeficiencies. Impaired vaccine-induced cell-mediated immunity was observed in many immunocompromised patients, particularly in solid-organ transplant and chronic lymphocytic leukemia patients. Notably, individuals with an inherited lack of mature B cells, i.e., X-linked agammaglobulinemia (XLA) displayed highly functional spike-specific T cell responses. Single-cell RNA-sequencing further revealed that mRNA vaccination induced a broad functional spectrum of spike-specific $CD4^+$ and $CD8^+$ T cells in healthy individuals and patients with XLA. These responses were founded on polyclonal repertoires of $CD4^+$ T cells and robust expansions of oligoclonal effector-memory $CD45RA^+$ $CD8^+$ T cells with stem-like characteristics. Collectively, our data provide the functional continuum of SARS-CoV-2-specific T cell responses post-mRNA vaccination, highlighting that cell-mediated immunity is of variable functional quality across immunodeficiency syndromes.

INTRODUCTION

SARS-CoV-2 mRNA vaccination has proven highly effective for reducing the incidence of symptomatic and severe COVID-19 (Polack et al., 2020). The generation of neutralizing antibodies (nAbs) has been identified as a strong correlate of protection following mRNA vaccination (Khoury et al., 2021). Nevertheless, current vaccines are based on the initial Wuhan SARS-CoV-2

sequence, whereas variants of concern (including B.1.617.2 and B.1.1.529) are known to partly subvert nAbs (Planas et al., 2021, 2022) and, to a lesser extent, T cell recognition (Gao et al., 2022). This has galvanized the need to gain a complete picture of adaptive immune responses that might form additional layers of protection from severe COVID-19. T cells serve as a critical component in establishing effective humoral and cell-mediated immunity in most infections. Both $CD4^+$ and $CD8^+$ T cell responses are induced following SARS-CoV-2 vaccination (Sahin et al., 2020) and have previously been shown to form long-lasting immunity following both yellow fever vaccination (Fuertes Marraco et al., 2015) and SARS-CoV-1 natural infection (Le Bert et al., 2020; Ng et al., 2016). Following the first dose of SARS-CoV-2 mRNA vaccination, spike-specific T cell responses arise before the emergence of nAbs and may contribute to the early protective efficacy observed already after one dose (Kalimuddin et al., 2021). Additionally, $CD4^+$ and $CD8^+$ T cells are necessary to generate protective antibody responses and control SARS-CoV-2 replication in the respiratory tract in murine and non-human primate models (Israelow et al., 2021; McMahan et al., 2021). These data highlight the need for effective vaccines to induce a complementary humoral and cell-mediated SARS-CoV-2-specific immune response to establish protection.

Although the mRNA-based BNT162b2 (Pfizer/BioNTech) and mRNA-1273 (Moderna) vaccines have proven to be highly effective in the general population (Baden et al., 2021; Polack et al., 2020), previous studies on immunocompromised populations have observed weaker or absent humoral immune responses after vaccination (Embi et al., 2021; Pimpinelli et al., 2021; Rahav et al., 2021). Individuals with primary or secondary immunodeficiencies (e.g., human immunodeficiency virus [HIV], hematological malignancy, and immunosuppressive treatments) also exhibit increased morbidity and mortality rates compared with immunocompetent individuals following SARS-CoV-2 infection (Shields et al., 2021). Nevertheless, the spectrum of immunodeficiencies most likely renders into differential responses following vaccination and whether immunodeficiency affects the maintenance of long-term memory responses is unknown. A previous immunological study in a cohort of multiple sclerosis (MS) patients undergoing anti-CD20 treatment has demonstrated that robust cell-mediated immune responses can arise in the relative absence of humoral immunity post-vaccination (Apostolidis et al., 2021). The possibility that different immunodeficient conditions might elicit differential humoral and cell-mediated immunity is of utmost interest, given that these states might offer insight into immune correlates of protection from severe COVID-19 in the scenario of breakthrough infections.

Our understanding of T cell responses following mRNA vaccination is relatively scarce compared with humoral immunity. Previous studies using conventional flow-cytometry analysis have indicated that mRNA vaccines rapidly mobilize an early $CD8^+$ T cell response after the first dose (prime) when both spike-specific $CD4^+$ T cells and nAbs are hardly detectable in the circulation (Oberhardt et al., 2021). Following a second dose, a robust spike-specific $CD4^+$ T cell response is induced, and this is generally of a higher magnitude than the $CD8^+$ T cell response (Guerrera et al., 2021; Mateus et al., 2021). Through conventional flow analysis, mRNA vaccination has been shown to polarize the $CD4^+$ T cell response primarily into a T helper 1 (Th1) (Sahin et al., 2020) and a T follicular helper (Tfh) cell (Painter et al., 2021) phenotype. Longitudinal analysis has further demonstrated that polyfunctional spike-specific $CD4^+$ and $CD8^+$ T cells, based on interferon-γ (IFN-γ), tumor necrosis factor (TNF), interleukin-2 (IL-2), and CD107a expression of stem cell memory (T_{SCM}: $CD45RA^+CCR7^+CD95^+$) and central memory (T_{CM}: $CD45RA^-CCR7^+$) phenotypes, persist up to 6 months after mRNA vaccination (Guerrera et al., 2021). Simple classifications of spike-specific and other antigen-specific $CD4^+$ and $CD8^+$ T cells into helper and memory subsets have traditionally been based on a few key chemokine receptors or cytokines. However, most antigen-experienced T cells are part of a continuum of cell states and phenotypes that creates a heterogeneous pool of clonotypes beyond classical Th and memory classifications. Through the use of next-generation secretome and single-cell sequencing technologies, it is possible to generate a deeper profile of the functional landscape of SARS-CoV-2-specific T cells and bring nuance to the definition of fixed $CD4^+$ and $CD8^+$ T cell archetypes (Kiner et al., 2021).

To fill this knowledge gap, we investigated the functional profile of SARS-CoV-2-specific T cells following mRNA-based BNT162b2 vaccination in healthy donors and across a spectrum of immunodeficiencies. Using conventional flow cytometry and secretome analysis, we show that many immunocompromised patient groups exhibit non-coordinated humoral and cell-mediated immune responses, which does not preclude the detection of SARS-CoV-2-specific T cell responses at 6 months post-vaccination. Additionally, our data indicate that certain immunocompromised patients, e.g., those with X-linked agammaglobulinemia (XLA), still elicit functional T cell responses despite the lack of mature B cells and antibody responses post-vaccination. Through a combined activation-induced sorting pipeline, we defined the single-cell functional landscape of spike-specific $CD4^+$ and $CD8^+$ T cell clonotypes in healthy individuals and those with an inherent lack of mature B cells—beyond traditional Th and memory cell characteristics. Our findings define the functional nature of spike-specific $CD4^+$ and $CD8^+$ T cell clonotypes following mRNA vaccination and demonstrate highly variable humoral and cell-mediated immunity across the range of immunodeficiency disorders.

RESULTS

The magnitude of SARS-CoV-2-specific T cell responses after mRNA vaccination differs across different immunocompromised states

To examine the impact of immunodeficiency on cell-mediated immunity to SARS-CoV-2 vaccination, we initiated a prospective open-label clinical trial (COVAXID, EudraCT, no. 2021-000175-37) to investigate the immunogenicity of the BNT162b2 vaccine across a broad spectrum of immunocompromised patients and healthy controls (HCs) (Bergman et al., 2021). In this clinical trial, we also collected peripheral blood mononuclear cells (PBMCs) from a subset of patients, including HCs (n = 44) and individuals with (1) primary immunodeficiency (PID) (n = 48), (2) HIV infection (n = 50), (3) post hematopoietic stem cell transplantation (HSCT) (n = 43), (4) post solid-organ transplantation (SOT) (n = 41), and (5) chronic lymphocytic leukemia (CLL) (n = 53) (Figure 1A; Table S1). All study participants had negative PCR tests at

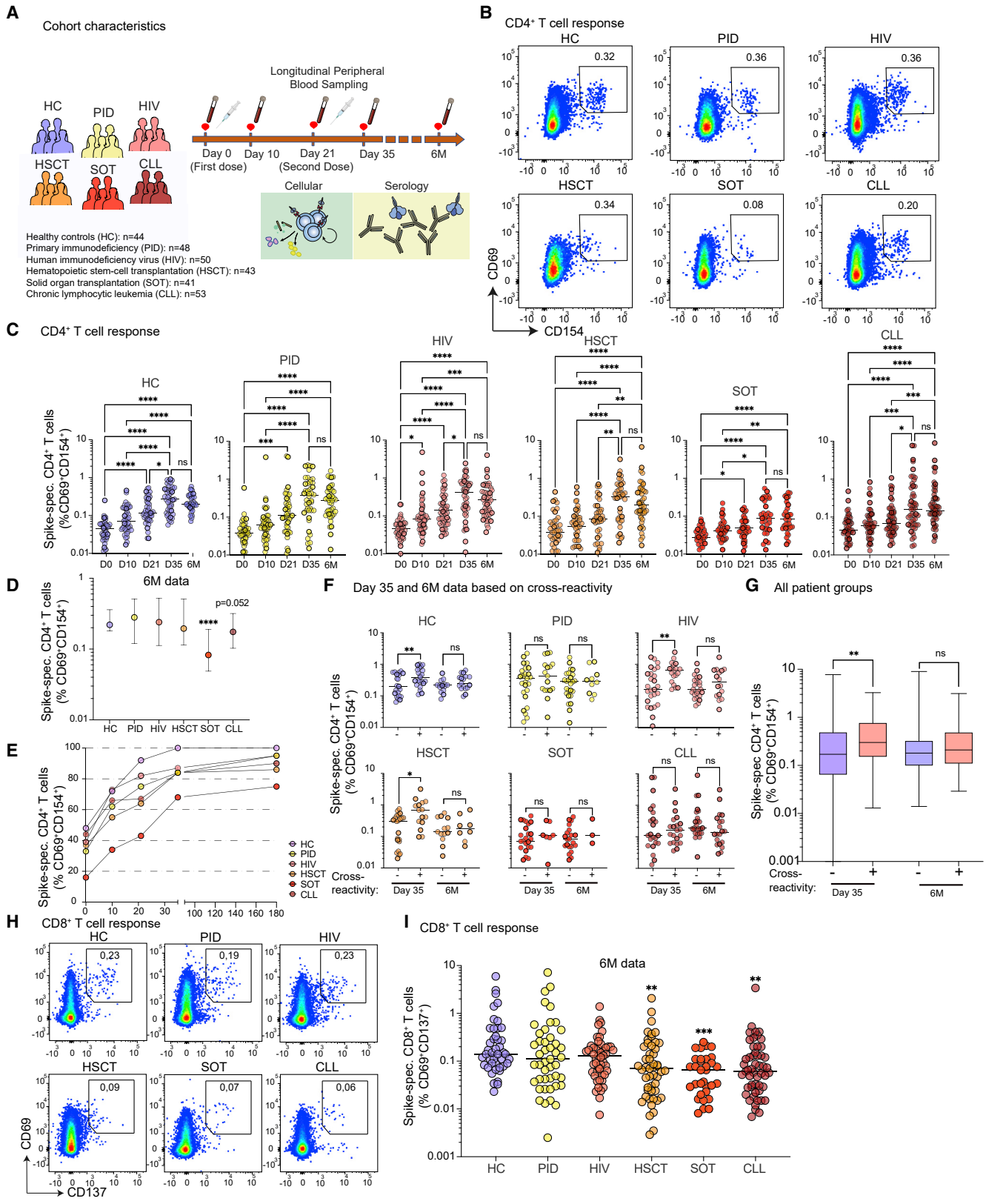

(legend on next page)

baseline and no previous documented COVID-19. Plasma and PBMCs were analyzed at five time points during vaccination (days 0, 14, 21, and 35 and 6 months) (Figure 1A).

We first tracked the longitudinal evolution of total T cell responses in all groups before and post-vaccination using IFN-γ ELISpot assay after overlapping SARS-CoV-2 spike-peptide pool stimulations. IFN-γ^+ T cell responses were undetectable in most donors prior to vaccination but increased after the first dose and continued to increase after the second dose (day 35) in all study groups (Figure S1A). On day 35, the CLL and SOT cohort showed the lowest fraction of detectable IFN-γ^+ responses (Figure S1A), where the magnitude of responses was significantly lower overall compared with HCs (Figure S1B).

To differentiate between $CD4^+$ and $CD8^+$ T cell responses, we next used spike-peptide pool stimulations and assessed activation-induced markers (AIMs), namely CD69 together with CD40L (CD154) for detection of vaccine (spike)-specific $CD4^+$ T cells and CD69 together with 4-1BB (CD137) to identify spike-specific $CD8^+$ T cells (Figure S1C). Most HCs responded rapidly to the first mRNA vaccine dose (day 10), and all showed detectable spike-specific $CD4^+$ T cells after two doses (day 35 and 6 months) (Figures 1B and 1C). Younger individuals (18–39 years) showed a trend toward higher frequencies of spike-specific $CD4^+$ T cells at day 35 but similar frequencies with elderly patient groups at 6 months (Figure S2A). The PID cohort responded well to the vaccine, particularly after the second vaccine dose (Figures 1B and 1C). All subjects with monogenic and other PIDs, followed by CD4 lymphopenia, common variable immunodeficiency (CVID), and XLA, had detectable spike-specific $CD4^+$ T cell responses at day 35 and 6 months (Figure S2B). Most HIV-infected patients generated positive $CD4^+$ T cell responses regardless of their infection stage (<300 cells/mm^3: 100%; >300 cells/mm^3: 83%) at day 35, which were maintained up to 6 months after vaccination (Figures 1B, 1C, and S2C). Most individuals undergoing HSCT displayed positive $CD4^+$ T cell responses at day 35 and 6 months (Figures 1B and 1C), although the time after HSCT influenced the response (Figure S2D). The SOT group showed a significant increase in $CD4^+$ T cell responses only after the second vaccine dose (Figures 1B and 1C). Particularly patients treated with mycophenolate mofetil (MMF) soon after transplantation had a notably poor $CD4^+$ T cell response (Figure S2E). Similarly, CLL patients produced significantly increased $CD4^+$ T cell responses only after the second vaccine dose (Figures 1B and 1C), where particularly patients with ongoing ibrutinib (a BTK inhibitor) treatment generated lower $CD4^+$ T cell responses (Figure S2F). At 6 months, the frequencies of spike-specific $CD4^+$ T cells were comparable between HC, PID, HIV, and HSCT, whereas SOT and CLL individuals exhibited significantly lower responses compared with HCs (Figure 1D). Overall, all HCs generated detectable spike-specific $CD4^+$ T cell responses at day 35 and 6 months, while more than one patient from each immunodeficiency group had undetectable responses (Figure 1E).

Pre-existing immunity correlates with increased SARS-CoV-2-specific $CD4^+$ T cell responses early after mRNA vaccination

Several studies have reported the existence of cross-reactive (pre-existing) T cells that recognize SARS-CoV-2 in peripheral blood and tissue (Braun et al., 2020; Grifoni et al., 2020; Niessl et al., 2021; Schulien et al., 2021; Sekine et al., 2020). Similar to these previous reports, we detected pre-existing $CD4^+$ T cells in 10%–40% of each patient group (Figure 1E). Notably, the SOT group, which responded poorly to the vaccine (Figure 1D), also displayed the lowest frequencies of pre-existing $CD4^+$ T cells (day 0) (Figure 1E). Individuals with pre-existing responses subsequently generated higher frequencies of $CD4^+$ T cell responses after the second vaccine dose at day 35, but not 6 months (Figure 1F). These data align with previous reports (Loyal et al., 2021). Still, here we also observed that pre-existing $CD4^+$ T cells were associated with improved spike-specific $CD4^+$ T cell responses across separate groups of immunodeficient patients (Figures 1F and 1G).

Immunocompromised patient groups generate variable magnitudes of SARS-CoV-2-specific $CD8^+$ T cell responses

We next assessed spike-specific $CD8^+$ T cells and found that these responses were induced post-mRNA vaccination (Figures 1H and S1C) but at lower frequencies than corresponding spike-specific $CD4^+$ T cells. Nevertheless, similar trends were observed, where the frequencies of spike-specific $CD8^+$ T cells were comparable between HC, PID, and HIV and lower in HSCT, SOT, and CLL individuals at 6 months (Figure 1I). In addition, we confirmed that the frequencies of IFN-γ^+ $CD8^+$ T cells were comparable between HC, PID, HIV, and HSCT and lower in SOT and CLL individuals at day 35 (Figure S1D).

Finally, we tested whether T cell responses against the Delta (B.1.617.2) variant were affected in individuals with PID or HCs. We observed no frequency differences between Delta and

Figure 1. Longitudinal T cell responses after SARS-CoV-2 mRNA vaccination in healthy controls and immunocompromised patients

(A) Schematic of the longitudinal study design, involving six cohorts of healthy and immunocompromised patient groups across five time points.

(B and C) (B) Representative flow plots at day 35 (n = 279 independent experiments) showing CD69 and CD154 expression after spike-peptide pool stimulation on memory $CD4^+$ T cells (above), and (C) plots of their frequencies over time (below).

(D) Spike-specific $CD4^+$ T cell frequencies at 6 months.

(E) Spike-specific $CD4^+$ T cell frequencies across all time points.

(F) Spike-specific $CD4^+$ T cell frequencies at ay 35 and 6 months based on the presence or absence of pre-existing day 0 responses.

(G) Spike-specific $CD4^+$ T cell frequencies at day 35 and 6 months based on the presence or absence of pre-existing day 0 responses with data combined from all individuals.

(H) Representative flow plots at 6 months (n = 279 independent experiments) showing CD69 and CD137 expression after spike-peptide pool stimulation of memory $CD8^+$ T cells.

(I) Spike-specific ($CD69^+CD137^+$) $CD8^+$ T cell frequencies at 6 months.

Graphs show median ± interquartile range (IQR) (D and G) or median values (C, F, and I). (C, D, and I) Kruskal-Wallis test with Dunn's post-test. (F and G) Mann-Whitney test. * $p< 0.05$, ** $p< 0.01$, *** $p< 0.001$, ns, not significant. See also Figures S1 and S2.

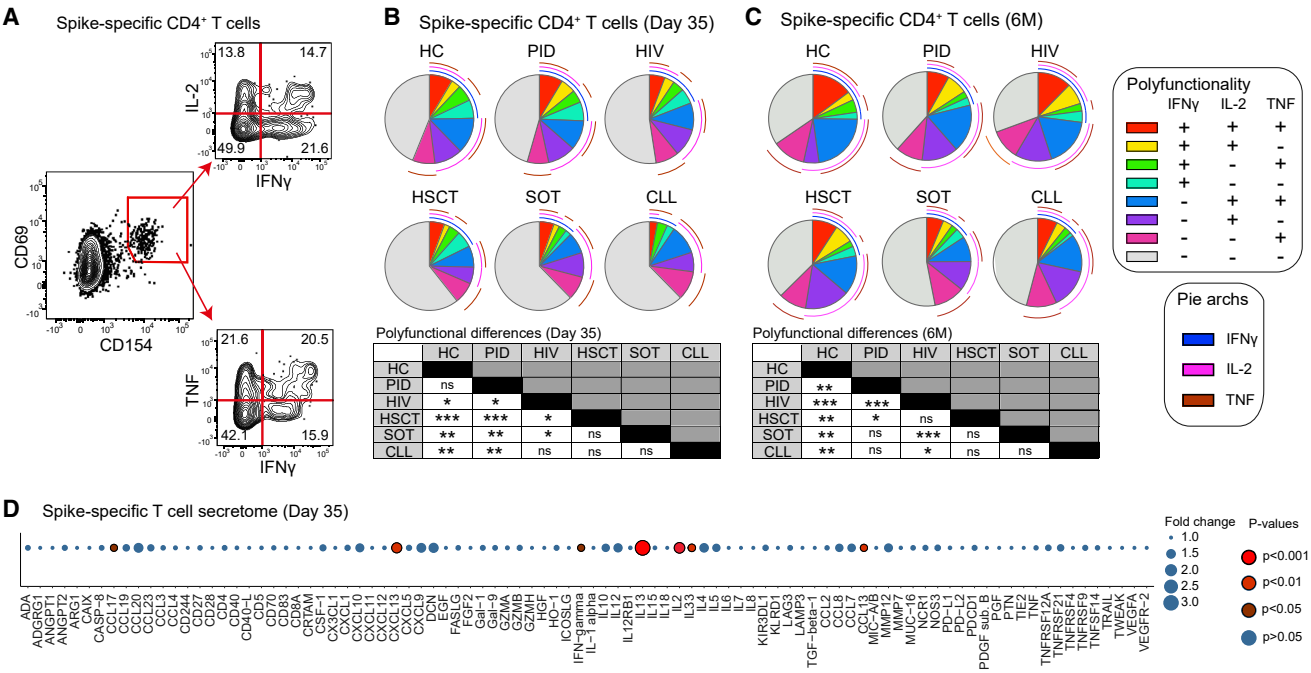

	HC	PID	HIV	HSCT	SOT	CLL
HC						
PID	ns					
HIV	*	*				
HSCT	***	***	*			
SOT	**	**	*	ns		
CLL	**	**	ns	ns	ns	

	HC	PID	HIV	HSCT	SOT	CLL
HC						
PID	**					
HIV	***	***				
HSCT	**	*	ns			
SOT	**	ns	***	ns		
CLL	**	ns	*	ns	ns	

Figure 2. Functional profile of spike-specific T cells

(A) Representative flow gating strategy (n = 279 independent experiments) for IFN-γ, IL-2, and TNF expression within the spike-specific CD4+ T cell population.

(B) Comparison of the co-expression pattern for IFN-γ, IL-2, and TNF molecules at day 35.

(C) Comparison of the co-expression pattern for IFN-γ, IL-2, and TNF molecules at 6 months.

(D) Bubble plot of the fold change over unstimulated background for secreted proteins after spike-peptide pool stimulation of PBMCs from day 35.

Graphs show median values (B–D). (B and C) Permutation test. (D) Mann-Whitney test between stimulated and unstimulated conditions. *p < 0.05, **p < 0.01, ***p < 0.001, ns, not significant. See also Figure S3.

wild-type spike-specific CD4+ and CD8+ T cells (Figure S2G). These data indicate that cell-mediated cross-recognition of Delta is not impacted to a high degree during immunodeficient states.

Immunodeficiency syndromes differentially impact the functional quality of SARS-CoV-2-specific T cells post-mRNA vaccination

To assess the functional features of spike-specific (CD69+ CD154+) CD4+ T cells, we combined the AIM assay with a polyfunctional assessment of IFN-γ, TNF, and IL-2 at day 35 and 6 months post-vaccination (Figure 2A). Few spike-specific CD4+ T cells expressed all cytokines together, and single or dual cytokine expression patterns differed between cohorts (Figures 2B and 2C). More specifically, the HC and PID groups experienced the highest spike-specific CD4+ T cell polyfunctionality, where IFN-γ was the least frequently expressed cytokine, particularly in the HIV, HSCT, SOT, and CLL groups at day 35 (Figures 2B and S3A). Increased polyfunctional characteristics of spike-specific CD4+ T cells were observed at 6 months post-vaccination, where HCs showed a diverse polyfunctional profile compared with all immunodeficient groups (Figures 2C and S3A).

Many spike-specific CD4+ T cells did not express IFN-γ, TNF, or IL-2 across the patient groups. We, therefore, expanded our functional T cell analyses by measuring the secretome of spike-peptide-stimulated PBMCs at days 0 and 35 with the Olink platform. On day 35, there was a marked increase in fold change of secreted molecules compared with the background cross-reactive secretome at day 0 (Figure 2D). This consisted of multiple cytokines and chemokines that distinguish Tfh, Th1, and Th2 polarized cells, including IL-13, IL-2, CXCL13, IL-4, and IFN-γ (Figure 2D). Additionally, CCL13 and CCL17 were significantly elevated compared with DMSO controls after spike stimulations, whereas other chemokines such as CCL20, CXCL19, and CXCL10 showed elevated tendencies (Figure 2D). To investigate the relative magnitude of protein secretion after spike stimulation, we compared the fold-change differences between the various patient groups and HCs. We detected a similar protein signature across all groups (Figure S3B). Collectively, our findings demonstrate that SARS-CoV-2 mRNA vaccination induces a functionally diverse T cell response in HCs and certain immunocompromised patient groups.

Healthy and immunocompromised individuals show discordant correlations between CD4+ T cell and antibody responses

CD4+ T cell help is essential for developing germinal center reactions and forming high-affinity antibodies (Crotty, 2011). We confirmed that the frequencies of spike-specific CD4+ T cells and antibody titers were positively correlated in all patient groups (Figure 3A). Notably, the CLL and SOT groups showed reduced antibody responses and displayed a poor correlation coefficient with spike-specific CD4+ T cells compared with the

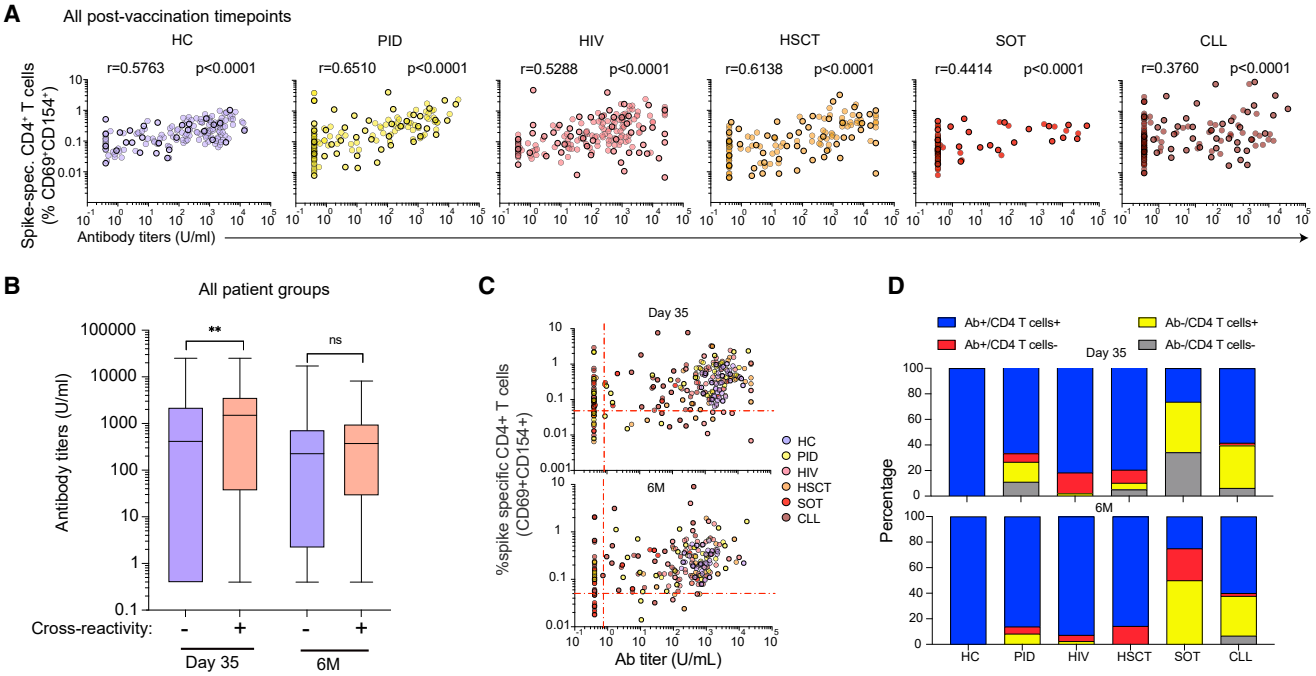

Figure 3. Relationship between spike-specific antibody and CD4$^+$ T cell responses after mRNA vaccination

(A) Correlative analysis of spike-specific antibody and CD4$^+$ T cell responses combined from all post-vaccination time points (days 10, 21, and 35 and 6 months).

(B) Distribution of spike-specific antibody titers based on the presence or absence of pre-existing (day 0) CD4$^+$ T cell responses.

(C) Scatter plot of spike-specific antibody titers and CD4$^+$ T cell response frequencies at day 35. Dashed lines represent the limit of detectable responses (antibody threshold = 0.8 U/mL, CD4$^+$ threshold = 0.05%, after background subtraction).

(D) The proportion of individuals with detectable antibody and/or spike-specific CD4$^+$ T cell responses at day 35 and 6 months.

Graphs show median ± IQR (B). (A) Spearman correlation. (B) Mann-Whitney test. * $p < 0.05$, ** $p < 0.01$, ns = not significant. See also Figure S3.

other groups (Figure 3A). Extending to our previous observations about the impact of pre-existing responses, we observed that HCs with pre-existing CD4$^+$ T cells produced higher antibody titers at day 35. This trend was not replicated in the immunocompromised groups and at a later point (6 months) across all cohorts (Figure S3C). Nevertheless, after pooling all groups together, we found that individuals with pre-existing CD4$^+$ T cells subsequently generated higher antibody titers at day 35 (Figure 3B).

We further examined discordant cell-mediated and humoral responses by comparing the proportion of individuals with detectable or undetectable spike-specific CD4$^+$ T cell and antibody responses at day 35 and 6 months post-vaccination across all cohorts. Only individuals within the HC group generated detectable spike-specific antibody and CD4$^+$ T cell responses, with variable humoral and cell-mediated immunity in the immunodeficient groups (Figure S3C). The CLL and SOT groups had the largest proportion of antibody-deficient vaccine responses at day 35 and 6 months (Figures 3C and 3D). Additionally, a lower fraction of detectable CD4$^+$ T cell responses when compared with humoral responses were observed in the HIV and HSCT groups at both day 35 and 6 months post-vaccination and in the SOT group at 6 months (Figures 3C and 3D). The PID group experienced heterogeneous humoral and cell-mediated response patterns depending on underlying conditions (Figures 3C and 3D). Notably, a fraction of individuals generated spike-specific CD4$^+$ T cell responses in the absence of detectable antibody responses, as exemplified by the XLA patients within the PID group who intrinsically lack mature B cells and the capacity to produce antibodies at day 35 (Figure S3D; Table S2). These data suggest that despite undetectable antibody responses, spike-specific T cell immunity may be efficiently formed after mRNA vaccination.

Longitudinal single-cell transcriptomics provides a high-resolution map of spike-specific T cells post-vaccination

Our observation that CD4$^+$ T cell responses could be generated in the absence of mature B cells prompted us to investigate the functional capacity of spike-specific T cell responses in the HC and XLA groups at day 35 (n = 6) and at 6 months (n = 5) post-vaccination. In this light, we used the 10X Genomics platform with 5′ V(D)J chemistry and a panel of oligo-conjugated antibodies (CD4, CD8, CCR7, CD45RA, and CXCR5) (Figure 4A) to perform single-cell sequencing on sorted spike-specific CD4$^+$ (CD69$^+$CD154$^+$) and CD8$^+$ (CD69$^+$CD137$^+$) T cells (n = 7,401 and n = 3,773 cells after quality control, respectively) (Table S3). Samples from the HC and XLA groups were stained, hashed, sorted (Figure S4A), and then sequenced. Cells with high mitochondrial content, low or high library sizes, co-expression of hashing antibodies, or co-expression of CD4 and CD8 were removed (Figure S4B). Louvain clustering and Uniform Manifold Approximation and Projection (UMAP) dimensionality reduction identified ten subsets consisting primarily of

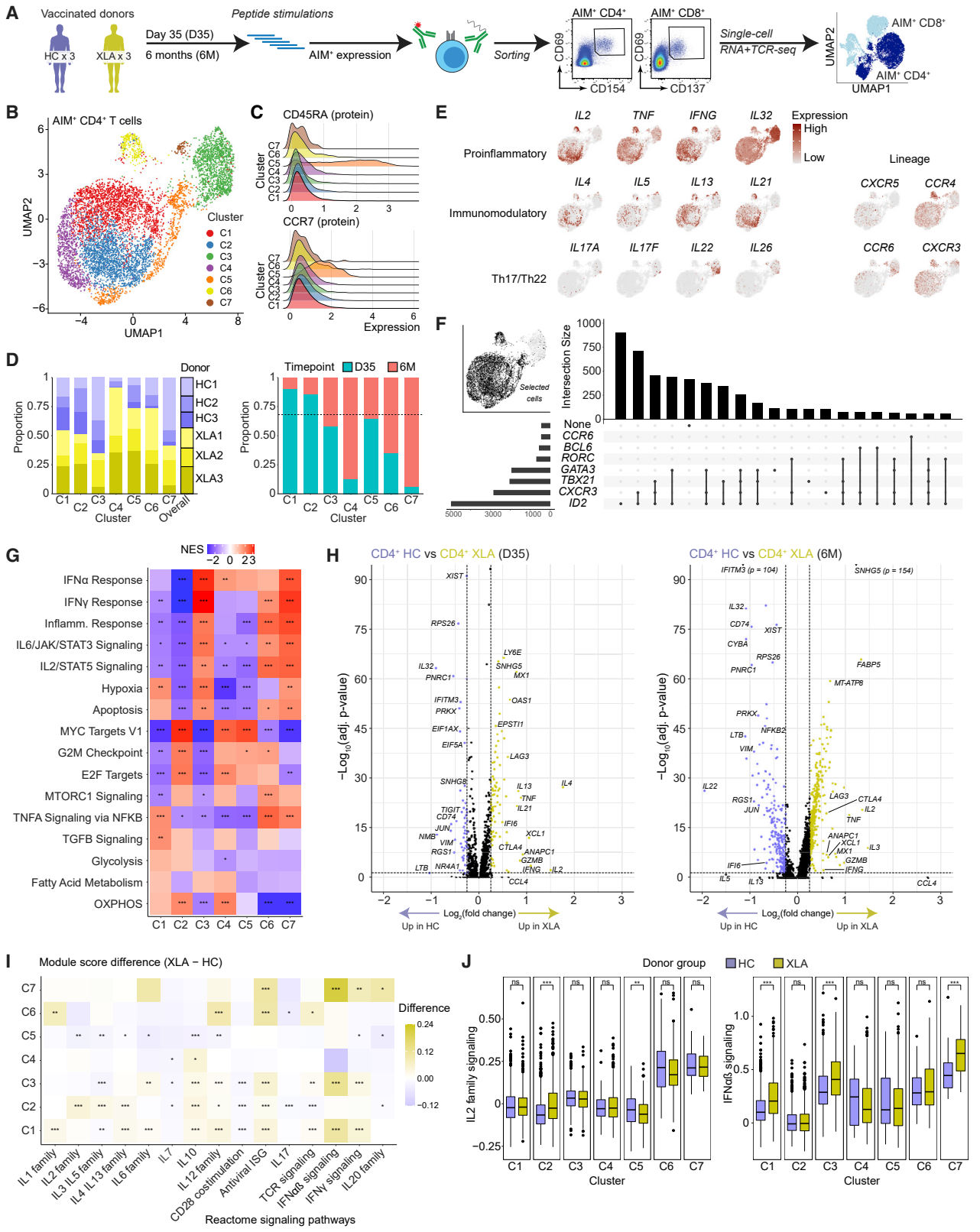

Figure 4. Single-cell transcriptome landscape of spike-specific CD4⁺ T cells in HCs and patients with XLA post-mRNA vaccination

(A) Schematic workflow for single-cell sequencing of spike-specific T cells.

(B) UMAP visualization of CD4⁺ T cell clusters (C1–C7) identified from HC and XLA patients at the day 35 and 6 months.

(legend continued on next page)

conventional CD4$^+$ and CD8$^+$ T cell phenotypes (Figures S4C and S4D). Localized regions in each cluster corresponded to a cell's donor or time point of origin (Figure S4E), but cells from multiple donors contributed to each cluster (Figure S4F). Within the CD8$^+$ compartment, we detected CD8-expressing unconventional (including $\gamma\delta$ T and NK cell) populations based on gene, T cell receptor sequencing, and protein signatures (Figures S4D, S4G, and S4H). For subsequent analyses in the CD8$^+$ compartment, we filtered based on marker gene expression and TCR identity to remove $\gamma\delta$ T, NK, NKT, and MAIT cell subsets (see STAR Methods).

mRNA vaccination generates a spectrum of functional CD4$^+$ T cell subsets in both HC and XLA donors

To evaluate the molecular phenotypes of spike-specific CD4$^+$ T cells, we selected only CD4$^+$ T cells by oligo-conjugated antibody staining. Seven clusters were identified (C1–C7) (Figure 4B), with distinct cytokine expression and memory phenotypes. Most clusters and donors were of a central- or effector-memory phenotype ($T_{CM/EM}$: CD45RA$^-$CCR7$^{+/-}$) (Figures 4C, S5A, and S5B), except for a T_{SCM} cluster (C5: CD45RA$^+$ CCR7$^+$) (Figure 4C; Table S4), which also expressed markers of memory cells (*FAS* and *IL2RB*) at frequencies similar to other clusters (Figure S5C). The 6-month time point populations from XLA donors were concentrated in cluster C4 (Figure 4D), with the remaining 6-month cells distributed throughout the other clusters (Figure S5D). Notably, the most highly enriched genes in C3 were *LTB*, *S100A4*, and *IL32* (Table S4) and were distinguished by a unique Th17 or Th22 cell cytokine profile, including *IL22* and *IL26* (Figure 4E). The remaining clusters were highly polyfunctional in their cytokine profile and expressed proinflammatory cytokines (*IL2*, *IFNG*, and *TNF*) but also detectable transcripts of immunomodulatory and Tfh- and Th2 cell-lineage cytokines (*IL4*, *IL5, IL13*, and *IL21*) in a continuous spectrum (Figure 4E). Inspection of lineage marker expression showed evidence for Th1- and Th2 cell- lineages (*CXCR3* and *CCR4*) (Figure 4E), whereas intracellular marker expression confirmed a stronger polarization of the Th1 cell lineage based on *ID2* expression (Figure 4F). Notably, Th1 polarized cells also co-expressed non-Th1 cell-lineage markers, including *GATA3* and *RORC* (Figure 4F), thus forming a spectrum of transcriptional states. Next, using the marker genes for each cluster, we applied gene set enrichment analysis (GSEA), which identified distinct pathway enrichment for IFN and inflammatory responses (in clusters C3, C6, and C7), which was contrasted by enrichment for cell cycling signatures (Myc targets and G2M checkpoint) (in clusters C2, C4, and C5), and TNFA and TGFB signaling in cluster C1 (Figure 4G).

Next, we directly investigated how XLA-immunodeficiency may impact CD4$^+$ T cell responses following mRNA vaccination compared with HCs. Patients with XLA demonstrated signatures enriched for functional Th1 or Th2 cell responses (*IL2*, *IFNG*, and *IL4*) (Figure 4H). Notably, these signatures were evident at both the day 35 and 6 month time points. Additionally, module scoring showed higher expression for Reactome pathways associated with IL signaling by patients with XLA (Figure 4I). These differences were particularly pronounced for IL-2 family signaling and IFN$\alpha\beta$ signaling for XLA donors in the largest clusters of C1 and C3, respectively (Figure 4J). Collectively, these data indicate that patients with XLA generated robust spike-specific CD4$^+$ T cells with similar to greater functionality than HCs.

XLA patients experience polyfunctional effector CD8$^+$ T cell responses post-vaccination

We further investigated conventional spike-specific CD8$^+$ T cell responses. Six clusters (C8–C13) were identified using Louvain clustering visualized by UMAP dimensionality reduction (Figure 5A; Table S5), using cells from XLA and HC donors at the day 35 and 6 month time points (Figure 5B). Most of each patient's response was dominated by the T_{EM} and effector-memory CD45RA$^+$ (T_{EMRA}) phenotypes with increasing proportions of the latter at the 6-month time point, particularly among patients with XLA (Figures S5E and S5F). To assess the functional capacity of the CD8$^+$ T cell response, we analyzed the transcriptional expression of a set of 12 effector-associated molecules (Zhang et al., 2020), which showed highly polyfunctional responses across all clusters (Figure 5C). Using GSEA (Hallmark pathways), the CD8$^+$ T cell clusters with the greatest functional responses were clusters C10, C11, and C13, enriched for IFN, inflammatory, and IL signaling, respectively (Figure 5D).

We next compared CD8$^+$ T cell responses between HCs and patients with XLA by investigating their phenotypic composition, effector responses, and activation status. Differential gene expression between the two patient groups confirmed that patients with XLA generated highly responsive CD8$^+$ T cells with comparable or higher expression for early activation molecules (*IL2RA*, *NME*1, and *IFIT3*) (Figure 5E; Szabo et al., 2019) and increased expression of effector transcripts (including *PRF1*, *IFNG*, *GNLY*, *GZMB*, and *GZMH*) (Figure 5F). We next scored the cytotoxic potential of patients with XLA and HCs by calculating the module scores for a set of cytotoxic genes (Figure 5C), which showed comparable or significantly higher cytotoxicity

(C) Ridge plots of CD45RA and CCR7 protein expression across CD4$^+$ T cell clusters.
(D) Bar plots of the composition of each cluster according to donor or time point of origin. The dotted line represents the overall distribution of cells between day 35 and 6 months.
(E) UMAP visualizations colored by gene expression intensity.
(F) UpSet plot of polarizing helper subset marker co-expression.
(G) Heatmap of normalized enrichment scores calculated using GSEA for Hallmark gene sets for each cluster. NES, normalized enrichment score.
(H) Volcano plot of differentially expressed genes between CD4$^+$ T cells from HC and XLA donors at the day 35 and 6-month time points. Genes with very low p values consisting only of sex-chromosome-linked genes were removed for visualization purposes.
(I) Heatmap showing the difference in median module scores between XLA and HC donors across clusters. Curated gene sets were obtained from the Reactome pathway database.
(J) Distribution of module scores for signaling pathways from the Reactome pathway database.
Graphs show median ± IQR (J). (G) GSEA permutation test. (I and J) Mann-Whitney test. (G, H, I, and J) *p < 0.05, **p < 0.01, ***p < 0.001, ns, not significant. See also Figures S4 and S5.

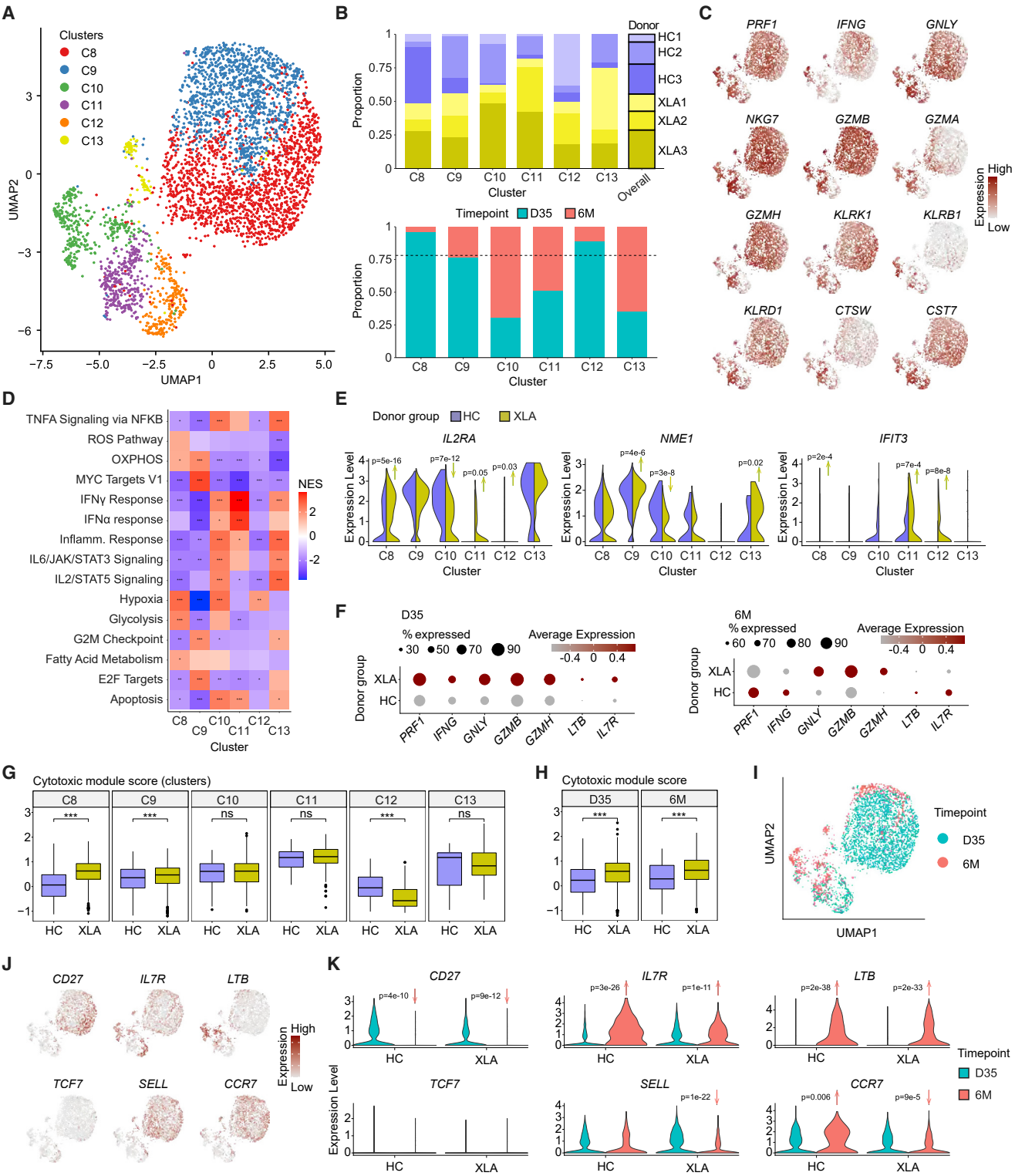

Figure 5. Single-cell analysis reveals the functional spectrum of spike-specific CD8⁺ T cell responses in HCs and XLA patients

(A) UMAP visualization of CD8⁺ T cell clusters (C8–C13) identified from HC and XLA donors at day 35 and 6 months. Day 35.

(B) Bar plots of the composition of each cluster according to donor or time point of origin. The dotted line represents the overall distribution of cells between day 35 and 6 months.

(C) UMAP visualizations for expression of a curated cytotoxic gene signature set colored by gene expression intensity.

(D) Heatmap of normalized enrichment scores calculated using GSEA for Hallmark gene sets for each cluster. NES, normalized enrichment score.

(legend continued on next page)

from XLA-patient-derived cells in most clusters (Figure 5G), and over time (Figure 5H).

We furthermore compared the transcriptome profile of spike-specific CD8$^+$ T cells between day 35 and 6 months. CD8$^+$ T cells at the two different time points were localized to distinct regions of the UMAP visualization (Figure 5I) and characterized by significantly higher transcript expression of the memory markers *IL7R* and *LTB* at 6 months (Figures 5J and 5K). XLA donors showed decreased *SELL* and *CCR7* transcript expression at 6 months (Figure 5K). Overall, our results demonstrate that mRNA vaccination induces polyfunctional and persistent spike-specific CD8$^+$ T cell responses in both HCs and patients with XLA, where the latter show robust cytotoxic capacity following anamnestic responses.

Clonality provides evidence for diverse recruitment and expansion of spike-specific T cells following vaccination

Our sequencing approach allowed us to characterize the clonal composition of total spike-specific CD4$^+$ and CD8$^+$ T cells between XLA and HC donors over time (Table S6). In the CD4$^+$ T cell compartment, Shannon's entropy diversity was not significantly different between the day 35 and 6 month time points and did not segregate by donor group (Figure S6A). Compositionally, the CD4$^+$ T cell repertoire was polyclonal, with few clones observed more than once (Figures S6B and S6C). The repertoire diversity in the CD8$^+$ T cell compartment was also highly similar over time (Figure S6D). However, the CD8$^+$ T cell repertoire was composed of multiple expanded clones, where the largest twenty clones typically accounted for half of the total population (Figure S6E). Furthermore, most clones were observed at least twice, with a single clone detected up to 107 times (donor HC3 at day 35) (Figure S6F). Collectively, mRNA vaccination mounts polyclonal repertoires of CD4$^+$ T cells and robust expansions of oligoclonal CD8$^+$ T repertoires in both XLA and HC donors.

Persisting CD8$^+$ T cell clones display a T_{EMRA} phenotype with stem-like traits

The presence of expanded CD8$^+$ T cell clones in both donor groups presented an opportunity to characterize the subset of identical clones identified at both day 35 and 6 months (Figure 6A). The largest clone at day 35 was no longer the predominant clone at 6 months (Figure 6B), suggesting that early clonal expansion does not necessarily predict the persistent spike-specific clonal landscape. Next, we compared protein expression of memory markers of shared clones at the day 35 and 6 month time points. We found increased CD45RA but unchanged CCR7 expression at the 6-month time point, indicating a transition into the T_{EMRA} phenotype (Figure 6C). Cells with shared clonotypes from both time points collectively shared phenotypic characteristics such as a tendency for co-localization in the same UMAP clusters, particularly cluster C3 (Figure 6D) and equivalent cytotoxic scores in four of the five donors (Figure 6E). Despite this fact, we observed an upregulation of specific functional (*IFNG, TNF, XCL1, XCL2, LTB,* and *LTA*) and memory transcripts (*IL7R, MYC,* and *BCL2L1*) at 6 months (Figure 6F), indicative of a polarized stem-like cytotoxic state. GSEA confirmed enriched effector and exhausted (activated) transcriptional signatures at day 35 compared with 6 months after vaccination. In contrast, the shared clones from the 6-month time point showed increased features of naive-like and memory traits (Figure 6G), despite the T_{EMRA} phenotype. In summary, our analyses demonstrate that both HC and XLA donors successfully generate memory CD8$^+$ T cell clonotypes that persist, to a high degree, as T_{EMRA} cells with combined cytotoxic and stem-like characteristics.

DISCUSSION

Coordinated humoral and cell-mediated immunity is critical for protection from viral disease. In contrast to antibody responses, however, the T cell arm remains relatively understudied after COVID-19 mRNA vaccination—particularly in patients with immunodeficiencies. Given that many of these individuals mount suboptimal B cell responses (Apostolidis et al., 2021; Bange et al., 2021), it remains essential to understand if these individuals can still generate effective cell-mediated immunity. These studies in immunocompromised states might be important and set the stage for future work identifying immune correlates of severe COVID-19 in breakthrough infections. In the present study, we addressed the impact of a broad range of immunodeficiencies on the longitudinal induction of T cell responses post-mRNA vaccination. We found that CLL and SOT patients notably elicited poor non-coordinated humoral and cell-mediated immune responses following two vaccination doses. In contrast, several immunocompromised patients, including patients with an inherited lack of mature B cells, mounted spike-specific T cells in the absence of antibody responses. Single-cell transcriptome analysis confirmed that individuals lacking B cells elicited robust clonotypic expansion of polyfunctional spike-specific CD4$^+$ and CD8$^+$ T cells following mRNA vaccination. These data provide a single-cell framework of anamnestic T cell responses following mRNA vaccination in a broad group of immunocompromised patients and indicate that individuals can mount highly functional T cell responses in the genetic absence of mature B cells.

Immunodeficient patients are disproportionally affected by severe COVID-19 (Fung and Babik, 2021) as well as relapsing and chronic SARS-CoV-2 infection (Brown et al., 2022). As such,

(E) Violin plots of gene expression for markers of activation.
(F) Dot plot of gene expression between all CD8$^+$ T cells from HC and XLA donors at day 35 and 6 months.
(G) Distribution of module scores for a cytotoxic gene signature across clusters.
(H) Distribution of module scores for a cytotoxic gene signature across time points.
(I) UMAP visualization for the time point of origin of cells.
(J) UMAP visualizations for expression of memory gene signatures colored by gene expression intensity.
(K) Violin plots of memory gene signatures split by time point and donor group of origin.
Graphs show median ± IQR (G and H). (D) GSEA permutation test. (E, G, H and K) Mann-Whitney test. (D, G, and H) * $p < 0.05$, ** $p < 0.01$, *** $p < 0.001$, ns, not significant. See also Figure S5.

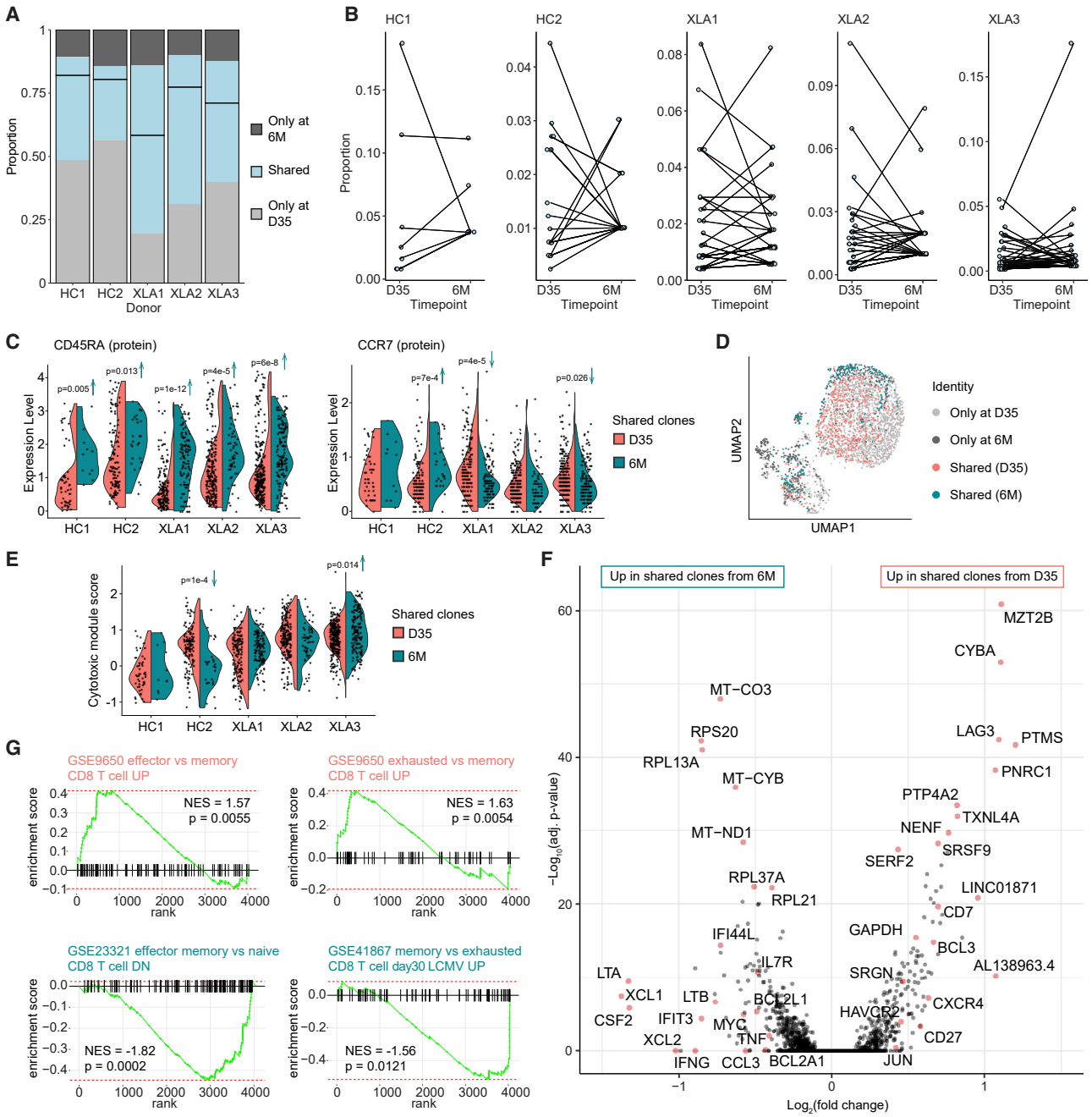

Figure 6. Phenotypic evolution of shared CD8⁺ T cell clones at 6 months post-vaccination

(A) Stacked bar plot of the proportion of the CD8⁺ T cell repertoire with paired clonotype (CDR3) identity from each donor observed at only one or both time points. The dividing line represents the contribution of clonotypes from each time point for each donor.

(B) Dot plot of the frequency of only cells with clonotype identity observed in both time points. Identical clonotypes are connected.

(C) Violin plots of the protein expression of CD45RA and CCR7 in cells with clonotype identity observed in both time points.

(D) UMAP visualization of the distribution of cells with clonotype identity observed in only two or both time points.

(E) Violin plot of the cytotoxic module score in cells with clonotype identity observed in both time points.

(F) Volcano plot of differentially expressed cells' genes from day 35 and 6 months with shared clonotypes.

(G) GSEA of C7 immunologic signature gene sets using the ranked set of differentially expressed genes between shared clonotypes from day 35 and 6 months.

(C, E, and F) Mann-Whitney test. (G) GSEA permutation test. See also Figure S6.

booster vaccinations have been prioritized for specific immunocompromised patient groups, where ongoing boosters might be needed in the future (e.g., for transplanted patients and those with certain hematologic malignancies). The findings from our study support this strategy, given that these patients, as well as many with CLL, show poor antibody and T cell responses

following two-dose mRNA vaccine regimens. Our observation that T cell responses in specific immunocompromised cohorts mirror the dynamics of healthy individuals over at least 6 months is promising given that other studies have shown waning protection (Naaber et al., 2021; Tartof et al., 2021), which may be rescued by booster vaccinations in healthy adults and result in lower rates of infection (Bar-On et al., 2021; Barda et al., 2021). Although SOT and CLL patients generally had suboptimal adaptive immunity compared to the other groups, we found that a fraction of these patients had detectable T cell responses in the absence of antibodies. As such, it will be of interest to further understand if detectable SARS-CoV-2-specific T cell responses, as described here, after two doses will be beneficial and serve as an immune correlate of improved antibody response in future booster studies of transplanted and other immunocompromised patient groups.

Previous studies have identified pre-existing T cells to SARS-CoV-2 in unexposed individuals (Braun et al., 2020; Grifoni et al., 2020; Niessl et al., 2021; Schulien et al., 2021). Recently, studies have also observed a correlation between pre-existing $CD4^+$ T cells and enhanced immune responses following SARS-CoV-2 infection and mRNA vaccination (Loyal et al., 2021; Mateus et al., 2020). We confirm these findings in HCs and demonstrate that pre-existing $CD4^+$ T cells to the spike antigen are associated with increased cell-mediated and humoral immunity across multiple immunodeficient states. We found that patients following SOT had the lowest frequency of pre-existing spike-reactive $CD4^+$ T cells compared with all other groups, which partly could explain the lower frequency of T cell responders in this group compared with the different cohorts. Whether the presence of pre-existing $CD4^+$ T cells is only an association or an actual link to increased B cell activation remains to be determined. Nevertheless, given that high numbers of virus-specific $CD4^+$ T cells and cognate Th functions promote germinal center reactions and increased B cell proliferation, it seems plausible that cross-reactive responses might enhance antibody responses. Further studies are needed to mechanistically determine if cross-reactive $CD4^+$ T cells can provide helper functions to improve antibody responses after mRNA vaccination.

In contrast to healthy individuals, we found that all immunocompromised patient groups had a certain degree of undetectable T cell or antibody responses. All patients with XLA belonged to this category with detectable T cell responses, except for one, despite the lack of antibody responses following mRNA vaccination. As such, these patients serve as a natural model to mechanistically dissect the human vaccine-induced T cell response in the absence of functional B cells. Our single-cell transcriptome data demonstrated that patients with XLA successfully generated $CD4^+$ and $CD8^+$ T cell responses of increased cytotoxic potential compared with healthy individuals. Furthermore, $CD8^+$ T cell clonotypes were characterized by a T_{EMRA} phenotype with memory characteristics at 6 months, suggesting the potential for long-term maintenance. These results were unexpected but in line with recent reports in MS patients treated with anti-CD20 (rituximab) (Apostolidis et al., 2021), highlighting future possibilities to generate neoantigen-based mRNA vaccination strategies in patients with B cell deficiencies. Previous case reports of patients with XLA have suggested that these patients can develop severe COVID-19. Nevertheless, they can resolve infections (Soresina et al., 2020), potentially through augmented T cell responses. The potential mechanism for increased cytotoxic $CD8^+$ T cell signatures in B cell deficiencies remains unknown. Still, it could be a consequence of a lack of antibody-mediated antigen clearance or diminished creation of immune complexes on dendritic cells (Li et al., 2014). Future studies of patients with XLA and other B cell deficiencies will be excellent models to fully understand how well vaccine-induced T cell responses can mediate protection from severe COVID-19.

The T cell receptor repertoire is relatively fixed following vaccination; therefore, future protection against emerging variants depends on recruiting sufficiently broad repertoires. Our study used a peptide pool covering the entire spike antigen, allowing us to identify the total spike-specific $CD4^+$ and $CD8^+$ T cell repertoire using combined single-cell transcriptome and clonotype analysis. Our results demonstrate that mRNA vaccination mounts a polyclonal repertoire of spike-specific $CD4^+$ T cells and a robust expansion of a relatively narrow cytolytic $CD8^+$ T cell clonal repertoire. These data may reflect a greater tendency for peptide stimulations to favor the detection of spike-specific $CD4^+$ T cells, as previous studies using multimer-based assays have shown high frequencies of SARS-CoV-2-specific $CD8^+$ T cells after infection (Saini et al., 2021). Nevertheless, through our combined approach with flow cytometry and single-cell sequencing, we could map the total spike-specific $CD4^+$ and $CD8^+$ T cell response—beyond traditional Th subsets or memory populations using conventional flow cytometry. Our single-cell data demonstrate that mRNA vaccination mounts a robust $CD4^+$ T cell response, segregated into continuous functional spectrums instead of discrete T helper subsets. For instance, the Th1 cell-biased response, as previously reported (Sahin et al., 2020), is also enriched for Th2 and Tfh cell signatures, whereas Th17 or Th22 cell-associated molecules are present in a unique cluster expressing *IL32*, *LTB*, and other memory markers. These results align with recent single-cell reports on antigen-specific $CD4^+$ T cells, showing a polarized continuity of transcriptional gradients rather than fixed Th archetypes (Kiner et al., 2021). The spike-specific $CD8^+$ T cell response also exhibited a profile of continuums with overlapping functions in different clusters that were highly heterogeneous between individuals and split between resting and highly cytotoxic responses. Our analysis of T cell responses at 6 months revealed a high degree of clonotypic maintenance in the $CD8^+$ T cell populations, as has been reported after infection (Adamo et al., 2022), and the development of a T_{EMRA} $CD8^+$ T cell phenotype characterized by increased expression of memory transcripts, including *IL7R* and *LTB*.

In summary, we here provide a profile of the total spike-specific $CD4^+$ and $CD8^+$ T cell responses following mRNA vaccination in healthy individuals and patients with different immunocompromising disorders. We show that mRNA vaccines induce a broad spectrum of highly active antiviral T cell clonotypes that aid in explaining how these vaccines generate protective responses against severe COVID-19 in healthy individuals. Our data also provide evidence of a highly heterogeneous mRNA vaccine response in immunocompromised patient groups, where patients with an inherited lack of mature B cells can still induce highly functional T cell responses in the absence of antibodies. Nevertheless, many immunodeficient patients show persistently reduced cell-mediated immunity and may need

future booster doses and prophylactic anti-SARS-CoV-2 monoclonal antibodies.

Limitations of the study

Our study contains several limitations. The study was designed to follow individuals over time to understand how various primary and secondary immunodeficiencies may differently impact immune responses to mRNA vaccination. As such, our cohort is highly heterogeneous, with differences in sex and age that may affect our results. Furthermore, this is a human study, and we cannot mechanistically study if T cell responses in the absence of antibodies can protect patients with B cell deficiencies from severe COVID-19. Future studies using T cell-based vaccines might be able to answer those questions. Finally, we have not assessed cross-reactive SARS-CoV-2-specific cell-mediated immune responses to Omicron. However, previous studies in immunocompetent individuals have found that established SARS-CoV-2-specific T cell responses can efficiently cross-recognize the Omicron variant (Gao et al., 2022; Keeton et al., 2022; Liu et al., 2022; Tarke et al., 2022), suggesting that similar results might be seen in immunocompromised patients.

STAR★METHODS

Detailed methods are provided in the online version of this paper and include the following:

- KEY RESOURCES TABLE
- RESOURCE AVAILABILITY
  - Lead contact
  - Materials availability
  - Data and code availability
- EXPERIMENTAL MODEL AND SUBJECT DETAILS
  - Study design
  - Human subjects and ethics
  - Peptides
- METHOD DETAILS
  - IFN-γ ELISpot assay
  - Serum protein quantification using proximity extension assay
  - Activation-induced marker (AIM) assay
  - Serology assay
  - Cell sorting
  - Single-cell RNA-sequencing
  - Data processing
  - Identification of unconventional subsets expressing CD8
  - Clustering and subset identification
  - Differential expression
  - Gene set enrichment
  - Module scoring
  - TCR analysis
  - Coexpression visualizations
  - Data analysis and statistics

SUPPLEMENTAL INFORMATION

Supplemental information can be found online at https://doi.org/10.1016/j.immuni.2022.07.005.

ACKNOWLEDGMENTS

This study has been funded by grants from the SciLifeLab National COVID-19 Research Program and financed by the Knut and Alice Wallenberg Foundation, the Swedish Research Council, Nordstjernan AB, Region Stockholm (Clinical research position-, ALF-, and CIMEDgrants), and a graduate student fellowship from Karolinska Institutet. In addition, the Swedish patient organizations of Primary Immunodeficiencies (PIO) and Hematology (Swedish Blood Cancer Foundation) provided grants. M.B. was supported by the Swedish Research Council, the Knut and Alice Wallenberg Foundation, the European Research Council, Karolinska Institutet, the Swedish Society of Medicine, the Swedish Cancer Society, the Swedish Childhood Cancer Fund, the Åke Wibergs Stiftelse, and the Jonas Söderquist Stiftelse. This work has partly been supported by NIH contract 75N9301900065 (A.S. and D. Weiskopf). J.N. was supported by an EMBO postdoctoral fellowship (ALTF 1062-2020). The authors acknowledge support from the National Genomics Infrastructure in Stockholm funded by Science for Life Laboratory, the Knut and Alice Wallenberg Foundation and the Swedish Research Council, and SNIC/Uppsala Multidisciplinary Center for Advanced Computational Science for assistance with massively parallel sequencing and access to the UPPMAX computational infrastructure.

AUTHOR CONTRIBUTIONS

Conceptualization, Y.G., C.C., J.K.S., C.I.E.S., P.B., H.-G.L., S.A., and M.B.; sample collection, O.R.-B., J.L., P.C., A.C., O.B., L.H., S. Mielke, P.N., M.A., A.P.-P., C.B., T.K., T.P., T.R.M., J.R.M., M.S., K.H., J.V., G.S., A.Ö., F.H., M.S.C., P.L., C.I.E.S., P.B., H.-G.L., S.A., and M.B.; investigation, Y.G., C.C., D. Wullimann., J.L., O.R.-B., G.B., S. Muschiol, S.A., and M.B.; formal analysis, Y.G., C.C., D. Wullimann, and S. Muschiol; visualization, Y.G., C.C., D. Wullimann, T.S., and M.B.; resources, A.G., D. Weiskopf, A.S., J.K.S., H.-G.L., S.A., and M.B.; funding acquisition, H.-G.L., S. Mielke, K.L., S.A., and M.B.; supervision, J.K.S., H.-G.L., S.A., and M.B.; writing—original draft, Y.G., C.C., and M.B.; writing—review and editing, C.C., J.N., and M.B.

DECLARATION OF INTERESTS

M.B. is a consultant for Oxford Immunotec. A.S. is a consultant for Gritstone, Flow Pharma, Arcturus, Immunoscape, CellCarta, Oxford Immunotech, and Avalia. A.S. has filed for patent protection for various aspects of T cell epitope and vaccine design work.

Received: December 16, 2021
Revised: May 5, 2022
Accepted: July 13, 2022
Published: July 19, 2022

REFERENCES

Adamo, S., Michler, J., Zurbuchen, Y., Cervia, C., Taeschler, P., Raeber, M.E., Baghai Sain, S.B., Nilsson, J., Moor, A.E., and Boyman, O. (2022). Signature of long-lived memory CD8+ T cells in acute SARS-CoV-2 infection. Nature *602*, 148–155.

Apostolidis, S.A., Kakara, M., Painter, M.M., Goel, R.R., Mathew, D., Lenzi, K., Rezk, A., Patterson, K.R., Espinoza, D.A., Kadri, J.C., et al. (2021). Cellular and humoral immune responses following SARS-CoV-2 mRNA vaccination in patients with multiple sclerosis on anti-CD20 therapy. Nat. Med. *27*, 1990–2001.

Baden, L.R., El Sahly, H.M., Essink, B., Kotloff, K., Frey, S., Novak, R., Diemert, D., Spector, S.A., Rouphael, N., Creech, C.B., et al. (2021). Efficacy and safety of the mRNA-1273 SARS-CoV-2 vaccine. N. Engl. J. Med. *384*, 403–416.

Bange, E.M., Han, N.A., Wileyto, P., Kim, J.Y., Gouma, S., Robinson, J., Greenplate, A.R., Hwee, M.A., Porterfield, F., Owoyemi, O., et al. (2021). CD8+ T cells contribute to survival in patients with COVID-19 and hematologic cancer. Nat. Med. *27*, 1280–1289.

Barda, N., Dagan, N., Cohen, C., Hernán, M.A., Lipsitch, M., Kohane, I.S., Reis, B.Y., and Balicer, R.D. (2021). Effectiveness of a third dose of the BNT162b2 mRNA COVID-19 vaccine for preventing severe outcomes in Israel: an observational study. Lancet *398*, 2093–2100.

Bar-On, Y.M., Goldberg, Y., Mandel, M., Bodenheimer, O., Freedman, L., Kalkstein, N., Mizrahi, B., Alroy-Preis, S., Ash, N., Milo, R., et al. (2021). Protection of BNT162b2 vaccine booster against Covid-19 in Israel. N. Engl. J. Med. *385*, 1393–1400.

Bergman, P., Blennow, O., Hansson, L., Mielke, S., Nowak, P., Chen, P., Söderdahl, G., Österborg, A., Smith, C.I.E., Wullimann, D., et al. (2021). Safety and efficacy of the mRNA BNT162b2 vaccine against SARS-CoV-2 in five groups of immunocompromised patients and healthy controls in a prospective open-label clinical trial. EBiomedicine *74*, 103705.

Borcherding, N., Bormann, N.L., and Kraus, G. (2020). scRepertoire: an R-based toolkit for single-cell immune receptor analysis. F1000Res *9*, 47.

Braun, J., Loyal, L., Frentsch, M., Wendisch, D., Georg, P., Kurth, F., Hippenstiel, S., Dingeldey, M., Kruse, B., Fauchere, F., et al. (2020). SARS-CoV-2-reactive T cells in healthy donors and patients with COVID-19. Nature *587*, 270–274.

Brown, L.K., Moran, E., Goodman, A., Baxendale, H., Bermingham, W., Buckland, M., Abdulkhaliq, I., Jarvis, H., Hunter, M., Karanam, S., et al. (2022). Treatment of chronic or relapsing COVID-19 in immunodeficiency. J. Allergy Clin. Immunol. *149*, 557–561.e1.

Conway, J.R., Lex, A., and Gehlenborg, N. (2017). UpSetR: an R package for the visualization of intersecting sets and their properties. Bioinformatics *33*, 2938–2940.

Crotty, S. (2011). Follicular helper CD4 T cells (TFH). Annu. Rev. Immunol. *29*, 621–663.

Embi, P.J., Levy, M.E., Naleway, A.L., Patel, P., Gaglani, M., Natarajan, K., Dascomb, K., Ong, T.C., Klein, N.P., Liao, I.C., et al. (2021). Effectiveness of 2-dose vaccination with mRNA COVID-19 vaccines Against COVID-19-associated hospitalizations Among immunocompromised adults - nine states, January–September 2021. MMWR Morb. Mortal. Wkly. Rep. *70*, 1553–1559.

Fuertes Marraco, S.A., Soneson, C., Cagnon, L., Gannon, P.O., Allard, M., Abed Maillard, S., Montandon, N., Rufer, N., Waldvogel, S., Delorenzi, M., and Speiser, D.E. (2015). Long-lasting stem cell-like memory CD8+ T cells with a naive-like profile upon yellow fever vaccination. Sci. Transl. Med. *7*, 282ra48.

Fung, M., and Babik, J.M. (2021). COVID-19 in Immunocompromised Hosts: What We Know So Far. Clin. Infect. Dis. *72*, 340–350.

Gao, Y., Cai, C., Grifoni, A., Müller, T.R., Niessl, J., Olofsson, A., Humbert, M., Hansson, L., Österborg, A., Bergman, P., et al. (2022). Ancestral SARS-CoV-2-specific T cells cross-recognize the Omicron variant. Nat. Med. *28*, 472–476.

Grifoni, A., Weiskopf, D., Ramirez, S.I., Mateus, J., Dan, J.M., Moderbacher, C.R., Rawlings, S.A., Sutherland, A., Premkumar, L., Jadi, R.S., et al. (2020). Targets of T cell responses to SARS-CoV-2 coronavirus in humans with COVID-19 disease and unexposed individuals. Cell *181*, 1489–1501.e15.

Guerrera, G., Picozza, M., D'Orso, S., Placido, R., Pirronello, M., Verdiani, A., Termine, A., Fabrizio, C., Giannessi, F., Sambucci, M., et al. (2021). BNT162b2 vaccination induces durable SARS-CoV-2 specific T cells with a stem cell memory phenotype. Sci Immunol. *5*, eabl5344.

Hao, Y., Hao, S., Andersen-Nissen, E., Mauck, W.M., 3rd, Zheng, S., Butler, A., Lee, M.J., Wilk, A.J., Darby, C., Zager, M., et al. (2021). Integrated analysis of multimodal single-cell data. Cell *184*, 3573–3587.e29.

Israelow, B., Mao, T., Klein, J., Song, E., Menasche, B., Omer, S.B., and Iwasaki, A. (2021). Adaptive immune determinants of viral clearance and protection in mouse models of SARS-CoV-2. Sci. Immunol. *6*, eabl4509.

Kalimuddin, S., Tham, C.Y.L., Qui, M., de Alwis, R., Sim, J.X.Y., Lim, J.M.E., Tan, H.C., Syenina, A., Zhang, S.L., Le Bert, N., et al. (2021). Early T cell and binding antibody responses are associated with COVID-19 RNA vaccine efficacy onset. Medicine *2*, 682–688.e4.

Keeton, R., Tincho, M.B., Ngomti, A., Baguma, R., Benede, N., Suzuki, A., Khan, K., Cele, S., Bernstein, M., Karim, F., et al. (2022). T cell responses to SARS-CoV-2 spike cross-recognize Omicron. Nature *603*, 488–492.

Khoury, D.S., Cromer, D., Reynaldi, A., Schlub, T.E., Wheatley, A.K., Juno, J.A., Subbarao, K., Kent, S.J., Triccas, J.A., and Davenport, M.P. (2021). Neutralizing antibody levels are highly predictive of immune protection from symptomatic SARS-CoV-2 infection. Nat. Med. *27*, 1205–1211.

Kiner, E., Willie, E., Vijaykumar, B., Chowdhary, K., Schmutz, H., Chandler, J., Schnell, A., Thakore, P.I., LeGros, G., Mostafavi, S., et al. (2021). Gut CD4(+) T cell phenotypes are a continuum molded by microbes, not by TH archetypes. Nat. Immunol. *22*, 216–228.

Le Bert, N., Tan, A.T., Kunasegaran, K., Tham, C.Y.L., Hafezi, M., Chia, A., Chng, M.H.Y., Lin, M., Tan, N., Linster, M., et al. (2020). SARS-CoV-2-specific T cell immunity in cases of COVID-19 and SARS, and uninfected controls. Nature *584*, 457–462.

Li, F., Smith, P., and Ravetch, J.V. (2014). Inhibitory Fcgamma receptor is required for the maintenance of tolerance through distinct mechanisms. J. Immunol. *192*, 3021–3028.

Liberzon, Arthur, Birger, Chet, Thorvaldsdóttir, Helga, Ghandi, Mahmoud, Mesirov, Jill P., and Tamayo, Pablo (2015). The Molecular Signatures Database Hallmark Gene Set Collection. Cell Systems *1*, 417–425.

Liberzon, Arthur, Subramanian, Aravind, Pinchback, Reid, Thorvaldsdóttir, Helga, Tamayo, Pablo, and Mesirov, Jill P. (2011). Molecular signatures database (MSigDB) 3.0. Bioinformatics *27*, 1739–1740. https://doi.org/10.1093/bioinformatics/btr260.

Liu, J., Chandrashekar, A., Sellers, D., Barrett, J., Jacob-Dolan, C., Lifton, M., McMahan, K., Sciacca, M., VanWyk, H., Wu, C., et al. (2022). Vaccines elicit highly conserved cellular immunity to SARS-CoV-2 Omicron. Nature *603*, 493–496.

Loyal, L., Braun, J., Henze, L., Kruse, B., Dingeldey, M., Reimer, U., Kern, F., Schwarz, T., Mangold, M., Unger, C., et al. (2021). Cross-reactive CD4(+) T cells enhance SARS-CoV-2 immune responses upon infection and vaccination. Science *374*, eabh1823.

Mateus, J., Dan, J.M., Zhang, Z., Rydyznski Moderbacher, C., Lammers, M., Goodwin, B., Sette, A., Crotty, S., and Weiskopf, D. (2021). Low-dose mRNA-1273 COVID-19 vaccine generates durable memory enhanced by cross-reactive T cells. Science *374*, eabj9853.

Mateus, J., Grifoni, A., Tarke, A., Sidney, J., Ramirez, S.I., Dan, J.M., Burger, Z.C., Rawlings, S.A., Smith, D.M., Phillips, E., et al. (2020). Selective and cross-reactive SARS-CoV-2 T cell epitopes in unexposed humans. Science *370*, 89–94.

McMahan, K., Yu, J., Mercado, N.B., Loos, C., Tostanoski, L.H., Chandrashekar, A., Liu, J., Peter, L., Atyeo, C., Zhu, A., et al. (2021). Correlates of protection against SARS-CoV-2 in rhesus macaques. Nature *590*, 630–634.

Naaber, P., Tserel, L., Kangro, K., Sepp, E., Jürjenson, V., Adamson, A., Haljasmägi, L., Rumm, A.P., Maruste, R., Kärner, J., et al. (2021). Dynamics of antibody response to BNT162b2 vaccine after six months: a longitudinal prospective study. Lancet Reg Health Eur. *10*, 100208.

Ng, O.W., Chia, A., Tan, A.T., Jadi, R.S., Leong, H.N., Bertoletti, A., and Tan, Y.J. (2016). Memory T cell responses targeting the SARS coronavirus persist up to 11 years post-infection. Vaccine *34*, 2008–2014.

Niessl, J., Sekine, T., Lange, J., Konya, V., Forkel, M., Maric, J., Rao, A., Mazzurana, L., Kokkinou, E., Weigel, W., et al. (2021). Identification of resident memory CD8(+) T cells with functional specificity for SARS-CoV-2 in unexposed oropharyngeal lymphoid tissue. Sci. Immunol. *6*, eabk0894.

Oberhardt, V., Luxenburger, H., Kemming, J., Schulien, I., Ciminski, K., Giese, S., Csernalabics, B., Lang-Meli, J., Janowska, I., Staniek, J., et al. (2021). Rapid and stable mobilization of CD8(+) T cells by SARS-CoV-2 mRNA vaccine. Nature *597*, 268–273.

Painter, M.M., Mathew, D., Goel, R.R., Apostolidis, S.A., Pattekar, A., Kuthuru, O., Baxter, A.E., Herati, R.S., Oldridge, D.A., Gouma, S., et al. (2021). Rapid induction of antigen-specific CD4(+) T cells is associated with coordinated humoral and cellular immunity to SARS-CoV-2 mRNA vaccination. Immunity *54*, 2133–2142.e3.

Pimpinelli, F., Marchesi, F., Piaggio, G., Giannarelli, D., Papa, E., Falcucci, P., Pontone, M., Di Martino, S., Laquintana, V., La Malfa, A., et al. (2021). Fifth-week immunogenicity and safety of anti-SARS-CoV-2 BNT162b2 vaccine in patients with multiple myeloma and myeloproliferative malignancies on active treatment: preliminary data from a single institution. J. Hematol. Oncol. *14*, 81.

Planas, D., Saunders, N., Maes, P., Guivel-Benhassine, F., Planchais, C., Buchrieser, J., Bolland, W.H., Porrot, F., Staropoli, I., Lemoine, F., et al. (2022). Considerable escape of SARS-CoV-2 Omicron to antibody neutralization. Nature *602*, 671–675.

Planas, D., Veyer, D., Baidaliuk, A., Staropoli, I., Guivel-Benhassine, F., Rajah, M.M., Planchais, C., Porrot, F., Robillard, N., Puech, J., et al. (2021). Reduced sensitivity of SARS-CoV-2 variant Delta to antibody neutralization. Nature *596*, 276–280.

Polack, F.P., Thomas, S.J., Kitchin, N., Absalon, J., Gurtman, A., Lockhart, S., Perez, J.L., Pérez Marc, G., Moreira, E.D., Zerbini, C., et al. (2020). Safety and efficacy of the BNT162b2 mRNA Covid-19 vaccine. N. Engl. J. Med. *383*, 2603–2615.

Rahav, G., Lustig, Y., Lavee, J., Ohad Benjamini, Magen, H., Hod, T., Noga Shem-Tov, Shmueli, E.S., Drorit Merkel, Ben-Ari, Z., et al. (2021). BNT162b2 mRNA COVID-19 vaccination in immunocompromised patients: a prospective cohort study. EClinicalmedicine *41*, 101158.

Roederer, Mario, Nozzi, Joshua L., and Nason, Martha C. (2011). SPICE: Exploration and analysis of post-cytometric complex multivariate datasets. Cytometry Part A *79*, 167–174. https://doi.org/10.1002/cyto.a.21015.

Sahin, U., Muik, A., Derhovanessian, E., Vogler, I., Kranz, L.M., Vormehr, M., Baum, A., Pascal, K., Quandt, J., Maurus, D., et al. (2020). COVID-19 vaccine BNT162b1 elicits human antibody and TH1 T cell responses. Nature *586*, 594–599.

Saini, S.K., Hersby, D.S., Tamhane, T., Povlsen, H.R., Amaya Hernandez, S.P., Nielsen, M., Gang, A.O., and Hadrup, S.R. (2021). SARS-CoV-2 genome-wide T cell epitope mapping reveals immunodominance and substantial CD8(+) T cell activation in COVID-19 patients. Sci. Immunol. *6*, eabf7550.

Schulien, I., Kemming, J., Oberhardt, V., Wild, K., Seidel, L.M., Killmer, S., Sagar, D.F., Salvat Lago, M., Decker, A., et al. (2021). Characterization of pre-existing and induced SARS-CoV-2-specific CD8(+) T cells. Nat. Med. *27*, 78–85.

Sekine, T., Perez-Potti, A., Rivera-Ballesteros, O., Strålin, K., Gorin, J.B., Olsson, A., Llewellyn-Lacey, S., Kamal, H., Bogdanovic, G., Muschiol, S., et al. (2020). Robust T cell immunity in convalescent individuals with asymptomatic or mild COVID-19. Cell *183*, 158–168.e14.

Shields, A.M., Burns, S.O., Savic, S., Richter, A.G., and Consortium, U.P.C. (2021). COVID-19 in patients with primary and secondary immunodeficiency: the United Kingdom experience. J. Allergy Clin. Immunol. *147*, 870–875.e871.

Soresina, A., Moratto, D., Chiarini, M., Paolillo, C., Baresi, G., Focà, E., Bezzi, M., Baronio, B., Giacomelli, M., and Badolato, R. (2020). Two X-linked agammaglobulinemia patients develop pneumonia as COVID-19 manifestation but recover. Pediatr. Allergy Immunol. *31*, 565–569.

Szabo, P.A., Levitin, H.M., Miron, M., Snyder, M.E., Senda, T., Yuan, J., Cheng, Y.L., Bush, E.C., Dogra, P., Thapa, P., et al. (2019). Single-cell transcriptomics of human T cells reveals tissue and activation signatures in health and disease. Nat. Commun. *10*, 4706.

Tarke, A., Coelho, C.H., Zhang, Z., Dan, J.M., Yu, E.D., Methot, N., Bloom, N.I., Goodwin, B., Phillips, E., Mallal, S., et al. (2022). SARS-CoV-2 vaccination induces immunological T cell memory able to cross-recognize variants from Alpha to Omicron. Cell *185*, 847–859.e11.

Tartof, S.Y., Slezak, J.M., Fischer, H., Hong, V., Ackerson, B.K., Ranasinghe, O.N., Frankland, T.B., Ogun, O.A., Zamparo, J.M., Gray, S., et al. (2021). Effectiveness of mRNA BNT162b2 COVID-19 vaccine up to 6 months in a large integrated health system in the USA: a retrospective cohort study. Lancet *398*, 1407–1416.

Zhang, J.Y., Wang, X.M., Xing, X., Xu, Z., Zhang, C., Song, J.W., Fan, X., Xia, P., Fu, J.L., Wang, S.Y., et al. (2020). Single-cell landscape of immunological responses in patients with COVID-19. Nat. Immunol. *21*, 1107–1118.

STAR★METHODS

KEY RESOURCES TABLE

REAGENT or RESOURCE	SOURCE	IDENTIFIER
Antibodies		
Anti-human CCR6 BUV737 (clone 11A9)	BD Biosciences	Cat# 612780; RRID:AB_2870109
Anti-human CCR7 APC-Cy7 (clone G043H7)	BioLegend	Cat# 353212; RRID:AB_10916390
Anti-human CD3 BUV805 (clone UCHT1)	BD Biosciences	Cat# 612895; RRID:AB_2870183
Anti-human CD4 FITC (clone SK3)	BD Biosciences	Cat# 566911; RRID:AB_2739682
Anti-human CD4 BUV496 (clone SK3)	BD Biosciences	Cat# 612936; RRID:AB_2870220
Anti-human CD8 BV711 clone (RPA-T8)	BioLegend	Cat# 301044; RRID:AB_2562906
Anti-human CD8 BUV395 (clone RPA-T8)	BD Biosciences	Cat# 563795; RRID:AB_2722501
Anti-human CD14 BV510 (clone M5E2)	BioLegend	Cat# 301842; RRID:AB_2561946
Anti-human CD19 BV510 (clone HIB19)	BioLegend	Cat# 302242; RRID:AB_2561668
Anti-human CD45RA BV570 (clone HI100)	BioLegend	Cat# 304132; RRID:AB_2563813
Anti-human CD69 BV650 (clone FN50)	BioLegend	Cat# 310934; RRID:AB_2563158
Anti-human CD69 BUV563 (clone FN50)	BD Biosciences	Cat# 748764; RRID:AB_2873167
Anti-human CD107A BV785 (clone H4A3)	BioLegend	Cat# 328644; RRID:AB_2565968
Anti-human CD137 (4-1BB) PE-Cy7 (clone 4B4-1)	BioLegend	Cat# 309818; RRID:AB_2207741
Anti-human CD154 (CD40L) BV421 (clone 24-31)	BioLegend	Cat# 310824; RRID:AB_2562721
Anti-human CD194 (CCR4) BV605 (clone 1G1)	BD Biosciences	Cat# 562906; RRID:AB_2737882
Anti-human CXCR3 BV750 (clone 1C6)	BD Biosciences	Cat# 746895; RRID:AB_2871692
Anti-human CXCR5 BB515 (clone RF8B2)	BD Biosciences	Cat# 564624; RRID:AB_2738871
Anti-human IFN-γ PE (clone B27)	BD Biosciences	Cat# 506507; RRID:AB_315440
Anti-human IL-2 PE-Dazzle594 (clone MQ1-17H12)	BioLegend	Cat# 500344; RRID:AB_2564091
Anti-human Ki67 AF647 (clone B56)	BD Biosciences	Cat# 558615; RRID:AB_647130
Anti-human CD38 APC-R700 (clone HIT2)	BD Biosciences	Cat# 564979; RRID:AB_2744373
Anti-human granzyme B BB790 (clone GB11)	BD Biosciences	Custom conjugate
Anti-human PD-1 BV711 (clone EH12.2H7)	BioLegend	Cat# 329928; RRID:AB_2562911
Anti-human CD40 primary antibody (clone HB14)	Miltenyi Biotec	Cat# 130-108-041; RRID:AB_2660897
Anti-human TNF-α BV650 (clone Mab11)	BD Biosciences	Cat# 502936; RRID:AB_2563884
TotalSeqC Anti-human CCR7 (clone G043H7)	BioLegend	Cat# 353251; RRID:AB_2800943
TotalSeqC Anti-human CXCR5 (clone J252D4)	BioLegend	Cat# 356939; RRID:AB_2800968
TotalSeqC Anti-human CD4 (clone RPA-T4)	BioLegend	Cat# 300567; RRID:AB_2800725
TotalSeqC Anti-human CD8 (clone SK1)	BioLegend	Cat# 344753; RRID:AB_2800922
TotalSeqC Anti-human CD45RA (clone HI100)	BioLegend	Cat# 304163; RRID:AB_2800764
TotalSeq-C0251 anti-human Hashtag 1	BioLegend	Cat# 394661; RRID:AB_2801031
TotalSeq-C0252 anti-human Hashtag 2	BioLegend	Cat# 394663; RRID:AB_2801032
TotalSeq-C0253 anti-human Hashtag 3	BioLegend	Cat# 394665; RRID:AB_2801033
TotalSeq-C0254 anti-human Hashtag 4	BioLegend	Cat# 394667; RRID:AB_2801034
Co-Stimulatory Antibodies (CD28/CD49d)	BD Biosciences	Cat# 347690; RRID:AB_647457
Biological samples		
Cryopreserved peripheral blood mononuclear cells	Bergman et al., 2021	EudraCT no. 2021-000175-37
Chemicals, peptides, and recombinant proteins		
BD Golgi Stop (with Monensin)	BD Biosciences	Cat# 554724; RRID:AB_2869012
Brefeldin A	BioLegend	Cat# 420601
Brilliant Stain Buffer Plus	BD Biosciences	Cat# 566385; RRID:AB_2869761
DNAse	Sigma-Aldrich	Cat# 4716728001
FoxP3/Transcription Factor Buffer Set	ThermoFisher Scientific	Cat# 00-5523-00

(*Continued on next page*)

Continued

REAGENT or RESOURCE	SOURCE	IDENTIFIER
LIVE/DEAD Fixable Aqua Dead Cell stain Kit	ThermoFisher Scientific	Cat# L34957
Paraformaldehyde	Biotium	Cat# 22023
RPMI-1640 without L-Glutamine	Cytiva	Cat# SH30096.01
SARS-CoV-2 Spike Peptide pools	Peptides & Elephants	UniProt: P0DTC2
Fetal bovine serum	Sigma-Aldrich	Cat# F7524
Penicillin-streptomycin	Cytiva	Cat# SV30010
L-glutamine	Sigma-Aldrich	Cat# 59202C
Critical commercial assays		
ELISpot Pro: Human IFN-γ kit	Mabtech	Cat# 3420-2APT-2
Elecsys Anti- SARS-CoV-2 S	Roche diagnostics	Cat# 09 289 267 190
Immuno-Oncology Olink panel	Olink	RRID:SCR_003899
Chromium Next GEM Single Cell 5' Library & Gel Bead Kit v1.1	10X Genomics	Cat# PN-1000165
Chromium Next GEM Chip G Single Cell Kit	10X Genomics	Cat# PN-1000120
Single Index Kit T Set A	10X Genomics	Cat# PN-1000213
Single Index Kit N Set A	10X Genomics	Cat# PN-1000212
Chromium Single Cell V(D)J Enrichment Kit, Human T Cell	10X Genomics	Cat# PN-1000005
Deposited data		
Processed single cell RNA-seq data	This paper	ArrayExpress: E-MTAB-11845
Software and algorithms		
FlowJo Version 10	BD Biosciences	RRID: SCR_008520
R (programming language)		RRID: SCR_001905
SPICE	Roederer et al., 2011	RRID: SCR_016603
Seurat R package	Hao et al., 2021	RRID:SCR_016341
ggplot2 R package		RRID:SCR_014601
Cell Ranger	10X Genomics	RRID:SCR_017344
Other		
Molecular Signatures Database (mSigDB) v7.5.1	Liberzon et al., 2011, 2015	RRID:SCR_016863

RESOURCE AVAILABILITY

Lead contact

Further information and requests for resources and reagents should be directed to and will be fulfilled by the lead contact, Marcus Buggert (marcus.buggert@ki.se).

Materials availability

This study did not generate any new unique reagents.

Data and code availability

The processed scRNA-seq data reported in this paper are available in the ArrayExpress database (http://www.ebi.ac.uk/arrayexpress) under accession number ArrayExpress: E-MTAB-11845.

All codes supporting the current study are available from the corresponding author on request.

EXPERIMENTAL MODEL AND SUBJECT DETAILS

Study design

The objective of this study was to characterize the SARS-CoV-2-specific T cells response following mRNA COVID-19 vaccination in healthy and immunocompromised individuals.

Human subjects and ethics

In this longitudinal study, healthy controls (n=44) and patients with primary immunodeficiency (PID, n=48), human immunodeficiency virus infection (HIV, n=50), hematopoietic stem cell transplantation (HSCT, n=43), solid organ transplantation (SOT, n=41), chronic lymphocytic leukemia (CLL, n=53) were recruited between March and June of 2021. Detailed patient characteristics have been

described elsewhere for the Covaxid study (Bergman et al., 2021). Plasma and PBMCs were collected immediately before the first vaccine dose (Day 0), ten days after the first vaccine dose (Day 10), immediately before the second vaccine dose (Day 21), fourteen days after the second vaccine dose (Day 35) and six months after the first vaccine dose (6 months). The trial was registered at EudraCT (no. 2021-000175-37) and clinicaltrials.gov (no. 2021-000175-37). The study was approved by the Swedish Medical Product Agency (ID 5.1-2021-5881) and the Swedish Ethical Review Authority (ID 2021-00451). PBMCs were isolated via standard density gradient centrifugation and cryopreserved in fetal bovine serum (FBS) containing 10% dimethyl sulfoxide (DMSO). Plasma samples were collected from all individuals and stored at −80°C.

Peptides

Peptide pool stimulations used 316 overlapping peptides (15-mers with 11 aa overlap) (Peptides&Elephants) from the entire SARS-CoV-2 spike glycoprotein (UniProt: P0DTC2). The spike peptide pool was reconstituted in DMSO (10–20 mg/ml), diluted to 100 μg/ml in PBS, aliquoted, and stored at −20°C. Peptides for the VOC analysis spanned the entire SARS-CoV-2 spike protein and corresponded to the ancestral Wuhan (wild type) sequence or the B.1.617.2 (Delta) variant. Peptides were 15-mers overlapping by 10 amino acids and were synthesized as crude material (TC Peptide Lab, San Diego, CA), reconstituted in DMSO, and diluted in PBS as described above.

METHOD DETAILS

IFN-γ ELISpot assay

Cryopreserved PBMCs were resuspended in complete medium (RPMI 1640 containing 10% FBS, 1% penicillin-streptomycin, and 1% L-glutamine) and rested for 3-4 hours prior to assay. All experiments were performed in duplicates with 2.5 x 10^5 PBMCs per well supplemented with purified anti-CD28 and CD49d (347690, BD Biosciences) at 0.15 μg/mL and stimulated with either spike glycoprotein peptide pool (0.5 μg/ml) or negative control containing PBS with DMSO (<1%). The assay was performed using pre-coated plates and reagents from a human IFN-γ ELISpotPRO kit (3420-2APT-2, Mabtech). PBMCs were stimulated for 20 hours in assay plates incubated at 37°C and 5% CO_2. Spots were counted using the automated IRIS ELISpot reader (Mabtech) and Apex software (Mabtech) using default settings. Visible artifacts were removed by masking. Results were expressed as spot forming units (SFUs) per million PBMCs, calculated by subtracting the mean negative control wells from the mean of spike peptide pool stimulation wells. A positive response after subtraction was determined by the median of all negative control wells + 2 standard deviations (>37 SFU/10^6 PBMCs). Results were excluded from analysis if the mean of duplicate negative control wells were >100 SFUs/10^6 PBMCs.

Serum protein quantification using proximity extension assay

Culture supernatants from Spike and negative control stimulations from the ELISpot assays were harvested immediately after the 20-hour stimulation (above) and stored at -80°C until sent for analysis. Ninety-two proteins from the Immuno-Oncology Olink panel were assessed using proximity extension assay technology (Olink AB) on 20 individuals from each group at Day 0 and a subset of each cohort group (13 PID, 9 HIV, 8 HSCT, 13 SOT, 6 CLL, 11 HC) at Day 35. One sample from Day 0 did not pass quality control and was excluded from the analysis.

Activation-induced marker (AIM) assay

Cryopreserved PBMCs were thawed quickly, resuspended in complete medium in the presence of DNase I (10 U/ml; Sigma-Aldrich), and rested at 1×10^6 cells/well in 96-well U-bottom plates (Corning) for 3 hours at 37°C. The medium was then supplemented with anti-CXCR5–BB515 (clone RF8B2; BD Biosciences), followed 15 min later by the spike peptide pool (0.5 μg/ml), and a further 1 hour later by brefeldin A (1 μg/ml; Sigma-Aldrich) and monensin (0.7 μg/ml; BD Biosciences). Negative control wells contained equivalent DMSO. After 9 hours, cells were washed in PBS supplemented with 2% FBS and 2 mM EDTA (FACS buffer) and stained with other chemokine receptors for 10 min at 37°C. Additional surface stains were performed for 30 min at room temperature in the presence of Brilliant Stain Buffer Plus (BD Biosciences). Viable cells were stained by exclusion using a LIVE/DEAD Fixable Aqua Dead Cell Stain Kit (Thermo Fisher Scientific). Cells were then washed in FACS buffer and fixed/permeabilized using a FoxP3 Transcription Factor Staining Buffer Set (Thermo Fisher Scientific). Intracellular stains were performed for 30 min at room temperature. Stained cells were washed in FACS buffer, fixed in PBS containing 1% paraformaldehyde (PFA; Biotium), and acquired using a FACSymphony A5 (BD Biosciences). Flow cytometry reagents are listed in STAR Methods key resources table. To address T cell responses against overlapping spike peptides from the WT and Delta variant, we conducted similar AIM measurements for surface molecules (CD69, CD154, and 41-BB) described below in the cell sorting section.

Serology assay

Serum samples were analyzed using the quantitative Elecsys® Anti-SARS-CoV-2 S assay (Roche Diagnostics) on the Cobas 8000 e801pro to detect antibodies to the SARS-CoV-2 spike protein receptor-binding domain (RBD). The detectable range is between 0.40 and 250 U/mL, with a cut-off for positive results at ≥ 0.80 U/ml. Positive samples with antibody titers of >250 U/mL were re-tested following a 1/10 dilution and, in applicable cases, a 1/100 dilution which increased the upper detection level to 25,000 U/ml (Bergman et al., 2021).

Cell sorting

Cryopreserved PBMCs were thawed quickly, resuspended in complete medium in the presence of DNase I (10 U/ml; Sigma-Aldrich), and rested at 3-5× 10^6 cells/well in 24-well plates (Corning) for 3 hours at 37°C. The medium was then supplemented with CD40 block (clone HB14; Miltenyi Biotec), followed 15 minutes later by the spike peptide pool (0.5 μg/ml). Negative control wells contained equivalent DMSO. After 12 hours, cells were washed in PBS, followed by viable staining with LIVE/DEAD Fixable Aqua Dead Cell Stain Kit (Thermo Fisher Scientific) for 10 minutes at room temperature. Cells were washed in PBS supplemented with 2% FBS, 2 mM EDTA (FACS buffer), and stained with two TotalSeq-C antibodies (anti-CCR7 clone G043H7 and anti-CXCR5 clone J252D4) (BioLegend) for 10 min at 37°C. Immediately after without washing, immunofluorescent-antibody staining (CD4, CD8, CD40L, CD69, CD14, CD19, 4-1BB), anti-human Hashtag antibody staining (clone LNH-94/2M2, BioLegend), and remaining TotalSeq-C antibody stainings (anti-CD45RA clone HI100, anti-CD4 clone RPA-T4, anti-CD8 clone SK1) (BioLegend) were performed for 30 minutes at room temperature in the presence of Brilliant Stain Buffer Plus (BD Biosciences). Stained cells were then washed, resuspended in FACS buffer, and sorted using an MA900 Multi-Application Cell Sorter (Sony Biotechnology) (Figure S4A). Cells from HC and XLA individuals within the same batch were pooled together, generating three individual sample sets in total.

Single-cell RNA-sequencing

Sorted cells were immediately loaded onto a Chromium Single Cell Chip (10x Genomics) with a target capture rate of ~5000 single cells. Captured mRNA and molecules from antibody-derived tags (ADTs) and hashtag oligos (HTOs) were converted to cDNA and pooled for Illumina sequencing according to the manufacturer's instructions for Chromium Next GEM Single Cell V(D)J 5' v1.1 library preparation. Two library pools were prepared, one containing all the gene expression products and a second library containing enriched TCR products and TotalSeq/hashtag products. Each library pool was sequenced on separate lanes of a single NovaSeq6000 SP100 flow cell with an 8-base index read and a 26-base read 1 containing barcodes and unique molecular identifiers (UMIs) and a 98-base read 2 containing transcript sequences to a depth of approximately 50,000 to 90,000 reads per cellular barcode.

Data processing

Sequencing read alignment to reference genome (version GRCh38), gene expression quantification, and TCR reconstruction was performed using the multi command in the Cellranger pipeline (10x Genomics, v6.1.1). Relevant barcode sequences were provided for the alignment and quantification of HTOs and ADTs. Expression data (gene, protein, and hashtag) were combined using the R package Seurat (v4.0.3) (Hao et al., 2021) with the Read10X function. Cells were removed if they contained more than 7% of reads aligned to mitochondrial genes or expressed fewer than 700 genes or more than 5700 genes. Transcript expression was normalized using the LogNormalize method implemented in Seurat's NormalizeData function. Expression for ADTs and HTOs were transformed using the CLR (centered log-ratio) method. HTO demultiplexing was performed using Seurat's HTODemux function. Cells were grouped into either the CD4 or CD8 compartments based on higher ADT expression. TCR data was imported using the import_vdj command from the djvdj R package. For cells with more than one reconstructed alpha or beta chain, additional chains were discarded to retain only a single alpha and a single beta chain with the highest expression. Cells were considered to belong to a common clonotype if their CDR3 amino acid sequences matched precisely.

Identification of unconventional subsets expressing CD8

We observed that some cells stained positive for the CD8 protein but were not conventional $CD8^+$ T cells. Clustering analysis identified two transcriptional clusters of γδ T cells and NK cells (Figure S4F). Unconventional CD8 expressing subsets were removed from $CD8^+$ T cell analyses according to the following criteria: NK cells (NK cluster), MAIT cells (*TRAJ33* paired with TRAV1-2 and TRBV20-1 or TRAV1-2 and *TRBV6*), γδ T cells (*TRDV1*$^+$ or *TRGV3*$^+$ or *TRGV9*$^+$) and invariant NKT cells ($TRAV10^+$ and $TRAJ18^+$).

Clustering and subset identification

Gene expression values were scaled and centered using the ScaleData function (Seurat), and highly variable genes were selected using the Seurat vst algorithm. Clusters were identified using the FindNeighbors function with 15 dimensions and the FindClusters function with the Louvain algorithm. Dimensionality reduction was performed using the UMAP algorithm, and clusters were named based on the top differentially expressed genes from a Wilcox rank-sum test.

Differential expression

Marker genes for each UMAP cluster and pairwise differential expression analyses were calculated using the FindAllMarkers and FindMarkers functions (Seurat) with logfc.threshold=0.01. Pairwise comparisons for individual markers between two groups were compared by the Mann-Whitney test implemented in the wilcox.test R function.

Gene set enrichment

Differentially expressed genes were ranked according to average $\log_2$ fold change values and used as input for gene set enrichment analysis (GSEA) with the fgsea command and fgsea R package (v1.18) with 5000 permutations. Hallmark and C7 immunologic signature gene sets were downloaded from the MSigDB.

Module scoring

Gene module scoring was performed using the AddModuleScore function (Seurat). Gene sets classified under the Reactome terms 'Signaling by Interleukins' and 'Adaptive Immune System' were downloaded from MSigDB. A manually curated gene set for $CD8^+$ T cell cytotoxicity was sourced from a recent study of total peripheral responses during COVID-19 (Zhang et al., 2020).

TCR analysis

TCR analyses were performed using the scRepertoire R package (v1.3.2) (Borcherding et al., 2020) and custom R commands. The proportion of repertoire space occupied by each clone was calculated using the clonalProportion function. Shannon's entropy was calculated using the following formula: $-\Sigma(\text{clonotype frequency} * \log_2(\text{clonotype frequency}))$.

Coexpression visualizations

Coexpression analyses visualized using UpSet plots were produced using the UpSetR R package (v1.4) (Conway et al., 2017).

Data analysis and statistics

Flow cytometry data were analyzed using FlowJo software version 10.7.1 (FlowJo LLC). The gating strategy is shown in Figure S1. Spike-specific T cell responses of >0.05% after background reductions were considered positive. Only responses assigned as positive based on these criteria were included in downstream analyses to limit the impact of background noise. Stimulation indices were only included if the calculations were based on >10 cells in each marker+ population. Statistical analyses were performed using Prism version 9 for macOS (GraphPad Software Inc.). Significance between two paired groups was assessed using the Wilcoxon signed-rank test, and significance between two unpaired groups was assessed using the Mann-Whitney test. Significance among three or more unpaired groups or among paired groups with missing values was assessed using the Kruskal-Wallis test with Dunn's post-test. Categorical variables were compared using Fisher's exact test.